UNIVERSIDAD NACIONAL AUTÓNOMA DE MÉXICO

PROGRAMA DE MAESTRÍA Y DOCTORADO EN INGENIERÍA

CENTRO DE INVESTIGACIÓN EN ENERGÍA

THREE DIMENSIONAL TEMPERATURE SIMULATION OF THE LAS TRES VÍRGENES GEOTHERMAL FIELD, BAJA CALIFORNIA SUR, MEXICO, FROM COOLING OF TWO MAGMA CHAMBERS.

TESIS

QUE PARA OBTENER EL GRADO DE

MAESTRO EN INGENIERÍA

ENERGÍA - FUENTES RENOVABLES DE ENERGÍA

P R E S E N T A:

ING. FERNANDO JAVIER GUERRERO MARTÍNEZ

DIRECTOR DE TESIS:

DR. SURENDRA PAL VERMA JAISWAL

2012

Universidad Nacional Autónoma de México
UNAM
Biblioteca Central
Dirección General de Bibliotecas de la UNAM

UNAM – Dirección General de Bibliotecas
Tesis Digitales
Restricciones de uso

DERECHOS RESERVADOS ©
PROHIBIDA SU REPRODUCCIÓN TOTAL O PARCIAL

Todo el material contenido en esta tesis esta protegido por la Ley Federal del Derecho de Autor (LFDA) de los Estados Unidos Mexicanos (México).

El uso de imágenes, fragmentos de videos, y demás material que sea objeto de protección de los derechos de autor, será exclusivamente para fines educativos e informativos y deberá citar la fuente donde la obtuvo mencionando el autor o autores. Cualquier uso distinto como el lucro, reproducción, edición o modificación, será perseguido y sancionado por el respectivo titular de los Derechos de Autor.

JURADO ASIGNADO:

Presidente:	Dr. Jorge A. Andaverde Arredondo
Secretario:	Dr. Surendra P. Verma
Vocal:	Dr. Eduardo González Partida
1er. Suplente:	Dr. Pandarinath Kailasa
2do. Suplente:	Dr. Octavio García Valladares

Lugar donde se realizó la tesis:

Centro de Investigación en Energía, Temixco, Morelos, México.

TUTOR DE TESIS:

Dr. Surendra P. Verma

FIRMA

Agradecimientos

A la Universidad Nacional Autónoma de México, especialmente al Centro de Investigación en Energía por la oportunidad y apoyo brindados para la realización de esta tesis.

A mi alma máter, la Universidad Autónoma Metropolitana, en particular a la unidad Iztapalapa, de donde obtuve la formación necesaria para emprender este proyecto.

Al Consejo Nacional de Ciencia y Tecnología (CONACyT), por brindarme el financiamiento para realizar mi tesis de maestría.

A los integrantes del Jurado que con sus valiosos comentarios me fue posible mejorar la calidad de este trabajo.

Un agradecimiento póstumo al Dr. Ignacio Torres Alvarado cuyos comentarios a los Capítulos 1 y 2 de esta tesis también fueron incluidos.

A CentroGeo por su apoyo en la preparación de los mapas.

A mi director de tesis, el Dr. Surendra P. Verma, por la oportunidad de emprender con él esta apasionante proyecto y por su paciencia y confianza brindadas en todo momento.

A mi familia, por su ejemplo y apoyo.

Contents

List of Tables

List of Figures

Resumen

Se propone un modelo numérico tridimensional (3D) que determina el campo de temperaturas en estado natural del sistema geotérmico Las Tres Vírgenes (LTV) mediante el emplazamiento y enfriamiento de dos cámaras magmáticas.

Aplicaciones previas de modelado acoplado de cámara magmática y yacimiento, realizadas con el modelo computacional TCHEMSYS (***T****hermal and* ***CHE****mical* ***M****odeling of a Volcanic-Geothermal* ***SYS****tem*), motivaron el desarrollo un nuevo modelo 3D más adecuado para el campo geotérmico LTV. El campo de temperaturas generado por el nuevo modelo se ajustó bien a las temperaturas de referencia que sea han estimado en el campo.

Esto se logró mediante una conceptualización detallada del sistema volcánico que incluye el emplazamiento de dos cámaras magmáticas, variaciones laterales de propiedades físicas y la consideración de la topografía del área geográfica en el modelo numérico.

La metodología se estructuró como sigue:

1. Se desarrolló un modelo conceptual del sistema volcánico LTV considerando régimen tectónico, geología estructural, eventos eruptivos, afloramientos y geocronología.

2. Se estudiaron dos aplicaciones del modelo TCHEMSYS a fin de identificar la causas que afectan la calibración de los modelos cámara magmática-yacimiento.

3. Se propuso y evaluó el nuevo esquema numérico 3D tomando en cuenta los resultados previos. La calibración del modelo se realizó tomando como referencia temperaturas estimadas de la formación reportadas en la literatura.

En los resultados de la simulación se observó que la cámara magmática correspondiente al complejo volcánico Las Tres Vírgenes tiene una mayor influencia en el área geotérmica, sin embargo, la presencia de la cámara de la caldera El Aguajito fue importante en la definición de los patrones de flujo de calor. Por otra parte, se estimó que las cámaras magmáticas tienen una profundidad de entre 3000 y 3500 m por debajo del nivel del mar, con un volumen total de entre 482 y 536 km^3.

La tesis se estructura en seis capítulos. Se presenta una introducción en el Capítulo 1. En el Capítulo 2 se platea un modelo conceptual del campo geotérmico LTV. En el Capítulo 3 se presentan aspectos generales del modelo TCHEMSYS y se estudian dos aplicaciones. En el Capítulo 4 se desarrolla el modelo numérico 3D para el campo geotérmico LTV. El análisis de resultados y conclusiones se presentan en los Capítulos 5 y 6, respectivamente.

Abstract

It is proposed a three-dimensional (3D) numerical model that determines the temperature field in natural state of the Las Tres Vrgenes geothermal system by means of the emplacement and cooling of two magma chambers.

Previous applications of magma chamber-reservoir modeling have been carried out with the computational model TCHEMSYS (***T****hermal and* ***CHE****mical* ***M****odeling of a Volcanic-Geothermal* ***SYS****tem*) and have motivated the development of a new 3D model suitable for the LTV geothermal field. The temperature field provided by the new numerical model had a good agreement with estimated temperatures in the geothermal field.

This was achieved by means of a detailed conceptualization of the volcanic system that includes the emplacement of two magma chambers, lateral variations of physical properties and the consideration of the topography of the geographic area in the numerical model.

The methodology was structured as follows:

1. It was developed a conceptual model of the LTV volcanic system considering tectonic regime, structural geology, outcropping geology, eruptive events and geochronology.

2. Two applications of the TCHEMSYS model were studied to understand the causes that affect the model calibration in the magma chamber-reservoir models.

3. It was proposed and evaluated the new 3D numerical scheme considering previous results. Static Formation Temperatures (SFT) reported in the literature were used for model calibration.

From the simulation results, it is inferred that the magma chamber related to the LTV volcanic complex has a major thermal influence in the geothermal area, however, the chamber related to the El Aguajito caldera is important for the heat flux patterns in the system. Chambers depth between 3000 and 3500 m and total chambers volume between 482 and 536 km^3 were also inferred.

This thesis is structured in six chapters. An introduction is presented in Chapter 1. A conceptual model of the LTV geothermal field is developed in Chapter 2. Some general aspects and two applications of TCHEMSYS model are studied in Chapter 3. In Chapter 4 the new 3D numerical simulation of the LTV geothermal field is developed. Analysis of results and conclusions are presented in Chapters 5 and 6, respectively.

Chapter 1

Introduction

Due to the geological characteristics of Mexico, the country has a vast reserve of geothermal energy. 2332 geothermal manifestations, spread all over Mexico, have been registered until the year 2005 [1]. The necessity of governments to increase the renewable energy supplies makes the research and development of geothermal energy a strategic element in the energy policy. In this context, a three-dimensional (3D) computational model for simulating the thermal regime of the Las Tres Vírgenes geothermal system is presented.

In latest decades, computational analysis has become an indispensable tool in many branches of science and engineering. This is because technical advances allow us to obtain input data easier than in the past. Furthermore, more efficient computational facilities permit us faster solutions to numerical models. Therefore, computational models provide low cost solutions for a variety of technological and scientific problems. In geosciences many researchers have reported applications, such as Hardy [2] who developed a 2D analysis of structural evolution of calderas, Perugini [3] who reported studies in magma mixing and convection, and Yoshiaki [4] who modeled magma ascent processes.

In geothermal energy, the applications are mainly concerned with reservoir simulation: O'Sullivan *et al.* [5] presented the state of the art of this research area. Some further studies were published by Noorollahi and Itoi [6], and Mottaghy *et al.* [7].

Three-dimensional reservoir simulation has become a common practice in the development of geothermal projects [5, 6, 7], but it was only a few years ago when an integrated magma chamber-reservoir simulation model, in three dimensions (3D), was pro-

posed by Verma and Andaverde [8]: TCHEMSYS (**T**hermal and **CHE**mical **M**odeling of a Volcanic-Geothermal **SYS**tem), an eight module program written in Fortran 90 that simulates the complete volcanic-geothermal system consisting of magma emplacement and formation of geothermal reservoir.

Two Mexican geothermal fields have been studied with this 3D model: the Los Humeros, Puebla, and La Primavera, Jalisco. In the former, a thermal-chemical analysis and a sensitivity analysis of the temperature to chamber depth and volume were developed [8, 9]. In the latter, the application consisted of a sensitivity analysis of temperature to chamber depth and volume along with geothermometric analysis for model calibration [10] (Appendix A).

These studies have produced valuable results with respect to chemical evolution of magma in the Los Humeros caldera and the relative importance of chamber depth and volume for the reservoir. However, a spacial scaling problem related with the large aspect ratio between the volumes of magma chamber and reservoir has been noticed. This problem is expressed in a deficient thermal coupling of the magma chamber-reservoir system which makes it difficult the calibration of the model, as may be observed in Verma *et al.* [10].

Taking account of this previous work, a new 3D computational model of conductive cooling is proposed for a third case study: the Las Tres Vírgenes (LTV) geothermal system. LTV geothermal field is the latest geothermal project developed in Mexico by the Federal Commission of Electricity (CFE). Therefore, there is an opportunity for contributing to the knowledge and development of a recent geothermal project that, to date, has been less studied than other geothermal fields in Mexico.

This new computational model has the purpose of reproducing the natural state thermal regime of the LTV geothermal field and constitute the main objective of this thesis. This proposal is intended to achieve a better calibration of the model with measured and estimated temperatures with respect to previous applications of the TCHEMSYS model.

In synthesis, the objectives of this thesis are stated as follows.

1. To define a detailed conceptual model of the volcanic field based on geological and

geochronological aspects and to create a data base of this model for further computational processing.

2. To develop a numerical model of emplacement and conductive cooling of the heat source of the LTV geothermal field that produces better calibration results with respect to previous applications of the TCHEMSYS model.

The conceptual model proposed in this thesis for the LTV geothermal field includes two magma chambers instead of only one used in the TCHEMSYS model. Spherical geometry and a new emplacement scheme to model the magma chambers is proposed in order to obtain more realistic heat flux patterns. The topography of the geographic area is also included in the conceptual and numerical model since it has an influence in the temperature distribution in shallow depths.

Chapter 2

Conceptual model of the Las Tres Vírgenes geothermal system

2.1 Introduction to the LTV geothermal field

The LTV geothermal field is located in the northern part of the state of Baja California Sur, about 33 km northwest of the town of Santa Rosalía (Figure 2.1). It is a Quaternary volcanic field related to the fault system that caused the opening of the Gulf of California [14]. Three volcanic complexes are identified, from oldest to younger [15]: the Reforma caldera, Aguajito caldera and LTV volcanic complex (Figure 2.1). The Aguajito caldera and LTV volcanic complex are two important volcanic structures of the field, however the latter has a larger thermal influence in the geothermal area.

Exploration activities were started in 1982; the development of the field began in 1986 with the drilling of well LV-2. The geothermal power plant started operations in 2001 with two 5 MWe condensation units [11].

To date, nine wells have been drilled along with three directional wells [11]. All of them are distributed in two zones (Figure 2.2): north and south; the production wells LV-1 and LV-5 and injection wells LV-2 (LV2-A)[1] and LV-8 are placed in the north zone;

[1]The wells in parentheses means directional well drilled in the same place of the corresponding vertical well.

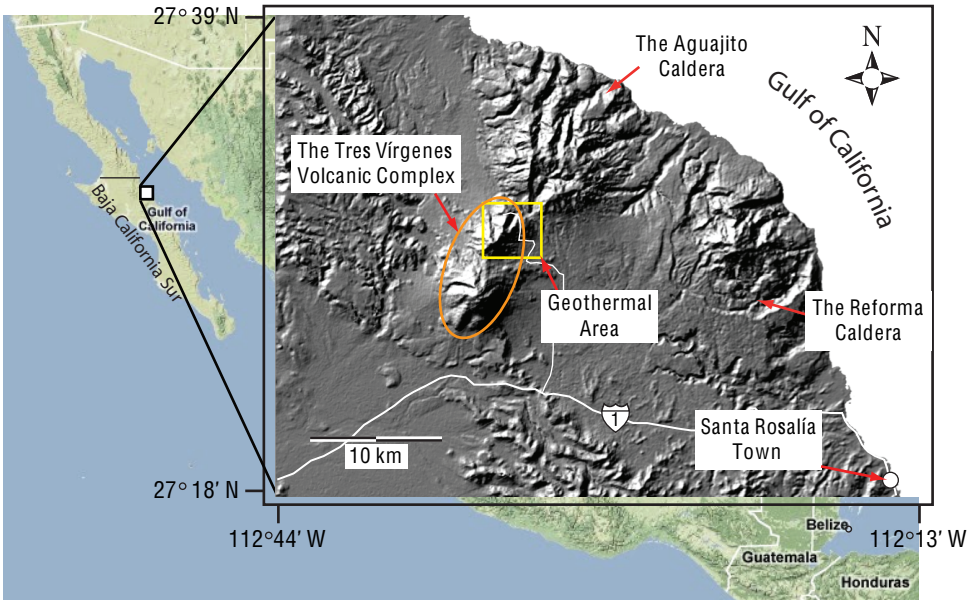

Figure 2.1: Location of the Las Tres Vírgenes Geothermal field. The geothermal area is shown in further detail in Figure 2.2.

wells LV-3, LV-4 (LV4-A), LV-13 (LV-13D), LV-11, and LV-7 are placed in the south zone, of which LV-11, LV-4A, LV-13D are production wells and LV-7 is an injection well. A liquid-dominated reservoir is located in a granodioritic intrusive basement between 950 and 1250 m of mean depth, it has temperatures in the range of 250-275 °C [11].

2.2 Geological Setting

The geology of the studied area has been reported in last decades by several authors (e.g. Demant and Ortlieb [12], Garduño-Monroy *et al.* [13], Capra *et al.* [14]). Geothermal exploration studies are summarized in Lopéz-Hernández [15]. Main aspects that permitted us to develop a conceptual model of the field are presented here.

The Tres Vírgenes geothermal area is located in a tectonically active zone. The ceaseation of subduction of Guadalupe plate beneath North America plate –from about 29 Ma to 12.5 Ma– led to a new extensional regime along with the transition of arc to rift volcanism. The opening of the Gulf of California and the origin of San Andreas fault

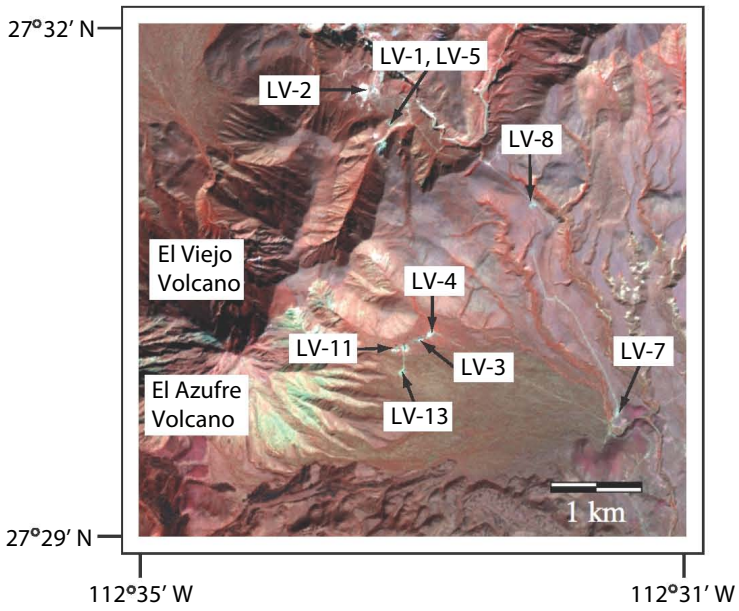

Figure 2.2: Geothermal area of the Las Tres Vírgenes geothermal field. The area is divided into two zones: north and south. In the north zone were drilled geothermal wells LV-1, LV-2, LV-5, and LV-8; in the south, wells LV-3, LV-4, LV-7, LV-11, and LV-13.

system resulted from this change in tectonic regime [16, 17, 18].

In late Miocene (10 Ma), a NE-SW to E-W extensive regime related to the opening of the present Gulf was started [15]. This led to a stepped NW-SE normal fault system descending towards the coast (La Virgen, El Azufre and El Viejo faults; Figure 2.3). As a consequence, the sea invaded low zones and the Santa Rosalía basin was formed. The deposition of marine sediments in this basin was controlled by the El Viejo fault which acted as a barrier causing the absence of sediments towards the SW of this fault [15].

Two eruptive centers were emplaced in the basin (about 6.5 Ma) during the deposition of sediments. These centers constitute the Reforma and Aguajito volcaninc complexes. The accumulation of sediments was interrupted periodically by tectonic movement related to the volcanic activity. Both volcanic centers were surrounded by sea until about 1 Ma [15].

The Reforma and Aguajito volcanic complexes had several eruptive periods [12, 13]. Pleistocene eruptive events are of particular interest for geothermal applications. Vol-

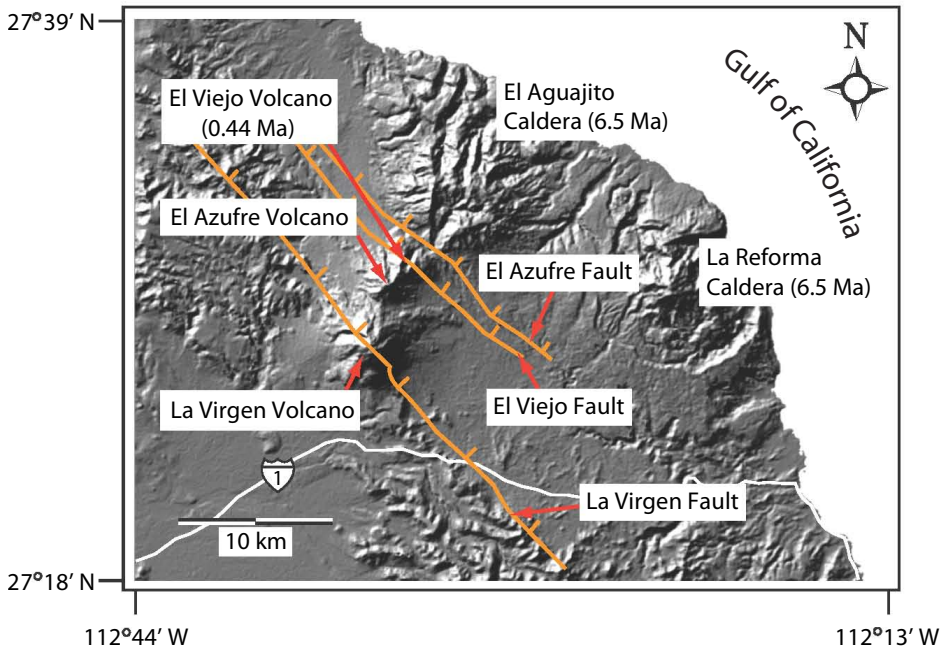

Figure 2.3: The Las Tres Vírgenes Geothermal field. The location of faults is from López-Hernández [15]. The approximated emplacement age of the volcanoes is provided. A plinian eruption of the La Virgen volcano (0.03 Ma) was the last eruption reported [14, 19].

canic activity in the Reforma caldera took place from late Pliocene (about 3.6 Ma) to early Pleistocene (about 0.8 Ma). At about 0.7 Ma, tectonic stresses made the eruptive activity to migrate towards NW reactivating the volcanism in the Aguajito caldera with the emission of Aguajito ignimbrite. The volcanic activity in this complex ended at about 0.5 Ma [15].

The development of a pull-apart system was started at the end of the cycle of the Aguajito. The La Virgen and El Azufre faults acted as the components of a shear stress. This regime led to the emplacement of the LTV volcanic complex formed by a chain of stratovolcanoes, from north to south: El Viejo, El Azufre, and La Virgen. The age of the edifices decrease from north to south. El Viejo volcano was emplaced at about 0.44 Ma and the last eruption of La Virgen volcano is dated at 0.03 Ma [19].

2.2.1 Lithology

The basement of the study area corresponds to a granodioritic intrusive body of about 91 Ma, which is a part of the Cretaceus batholith of the Baja California Peninsula [15]. A volcano-clastic sequence overlies this intrusive body. It is divided into two main parts: the oldest Comondú Group with mainly andesitic composition and the Santa Lucía Formation that overlies the Comondú Group. The composition of the Santa Lucía Formation is also andesitic but minor basalt and dacite are also present [15]. Surficial deposits correspond to andesite and dacite of the Azufre and the Viejo volcanoes.

As mentioned previously, the El Viejo fault functioned as a barrier to the deposition during the period of the Santa Rosalía basin (about 10 to 1 Ma) [15]. This inference may be confirmed from the lithology of wells LV-2 and LV-3 (Table 2.1) located in the north and south zones of the geothermal area, respectively (Figure 2.2).

This description implies that there are lateral variation in the physical properties of rocks in this geothermal field. The thermal diffusivity data corresponding to the conceptual model will be defined after the 3D spatial domain has been established in Section 2.4.

Table 2.1: Simplified lithology from two geothermal wells: LV-2 [20] and LV-3 [21].

Well	Layer	Depth interval (m)
LV-2	Surficial deposits	0-256
722 m a.s.l.	Sediments Santa Rosalía basin	256-356
Depth: 1142 m	Santa Lucía formation	356-695
	Comondú Group	695-1100
	Basement	1100-1142
LV-3	Surficial deposits	0-160
720 m a.s.l.	Santa Lucía formation	160-650
Depth: 2150 m	Comondú group	650-899
	Basement	900-2150

2.3 Geological events considered in the conceptual model

Taking into account the geological processes mentioned in Section 2.2, the conceptual model of the geothermal field was defined to comprise of reactivation of volcanism in the Aguajito until the present. This implies a temporal domain of 0.7 Ma. The Reforma caldera is not considered in this model because its eruptive activity ended long ago (at about 0.8 Ma), resulting in only a minor thermal influence.

A re-injection process was considered in connection with the last eruption of the La Virgen volcano (0.03 Ma). This assumption is based on Capra *et al.* [14] who showed evidence of mixing of basaltic and rhyolitic magmas before the eruption. The beginning of this re-injection process was assumed to start, tentatively, at 0.04 Ma. This time, and the re-injected volume, were defined as variables in the computational model (Chapter 4).

The process of formation of the geothermal reservoir was modeled by a gradual increase of conductivity below the reservoir up to a factor of 12. This is because a numerical model of convection in a porous-fractured medium would require a temporal discretization considerably smaller than that required for the chamber cooling, since these processes occur with different rates of energy transfer. The conductive scheme was used as an approximation to the actual convective heat transfer. Table 2.2 summarizes the geological events that were considered in this conceptual model.

Since the initial topography of the area is unknown, an initial topography of 0 m a.s.l.

Table 2.2: Geological events considered in the conceptual model.

Time b.p. (Ma)	Geological events
0.04	Re-injection processes in the LTV
0.05	Formation of the reservoir
0.44	Emplacement of the LTV volcanic complex
0.5	End of the El Aguajito activity
0.7	Emplacement of the El Aguajito

was assumed for the entire area. It is supposed that the elevation has grown linearly with the time, from 0.7 Ma to 0.03 Ma (a period of 0.67 Ma), the age of the last eruption [19]. Equation 2.1 shows this topographic growing scheme, the elevation at time t (Ma) is $h(x, y, t)$, and $E(x, y)$ is the present elevation. It is known, considering the geological history of the area, that the initial elevation at 0.7 Ma was different from zero. Because the value of zero was assumed for the present model, this initial topography was defined as a variable in the computational model for further sensitivity analysis.

$$h(x, y, t) = E(x, y) * \frac{t}{0.67} \qquad t \in [0, 0.67] \text{ Ma} \tag{2.1}$$

2.4 Domain of study

The domain of study was chosen assuming that the Aguajito Caldera and LTV volcanic complex are the volcanic systems that influence the geothermal area. A rectangular coordinate system (x, y) of 20000×30000 m was selected for delimiting the area of study (Figure 2.4).

For z coordinate, 20000 m b.s.l. were considered along with the addition of the maximum elevation that corresponds to La Virgen volcano: 1923 m a.s.l.. So that $z \in [0, 21923]$ with $z = 20000$ m corresponding to the sea level (Figure 2.5).

Since the surface is the primary reference for inferring subsurface structures, the surface characteristics were first defined. A uniform mesh with control volumes of 250×250 m was selected for mapping the surface. The mesh so defined contains 80×120=9600 control volumes for data sampling.

2.4.1 Topography and outcropping geology

After the mesh was defined, the outcropping geology and elevation a.s.l. were mapped and the resulting database was processed. In this work the geological map of López-Hernández [15] and the free software Google Earth for the elevation were used.

Figure 2.6 shows modeled outcropping geology of the volcanic area. Outcrops of the LTV and Aguajito were of particular interest in this work for estimating the eruptive

Figure 2.4: Rectangular coordinates system selected for delimiting the study area: $x \in [0, 20000]$, $y \in [0, 30000]$. The LTV volcanic complex and the Aguajito caldera are delimited for mapping eruptive products of the volcanic complexes (Figure 2.6) and the elevation (Figure 2.7). Section A-B ($x = 10000$) is shown in Figure 2.5 .

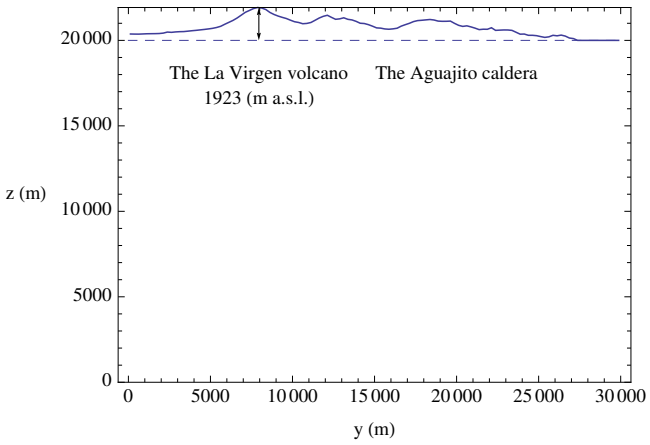

Figure 2.5: Cross section A-B (Figure 2.4), $x = 10000$ m, illustrating z domain, $z \in [0, 21923]$. Solid curve is the present elevation. Dashed line is the modeled initial topography correspondig to the sea level.

volumes and chamber volumes.

With respect to the topography, a text file was prepared with the elevation corresponding to the center of each control volume on the surface. The resulting discretized

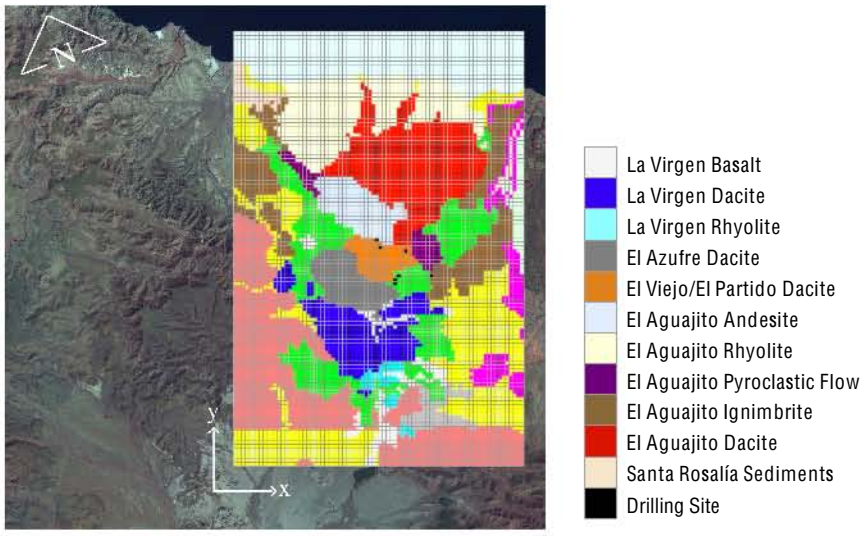

Figure 2.6: Outcropping geology of the LTV geothermal field, from López-Hernández [15]. Outcrops of the Aguajito and LTV volcanic complexes are shown in the figure key. Drilling sites are shown for reference.

topography is shown in Figure 2.7. Mean elevation of the geothermal area is about 700 m a.s.l..

A small influence of the sea in the model is expected, since there is a small aspect ratio between the deepest values of the sea (about 200 m) to all z domain (21923 m). Because of this consideration, the sea was assumed to be part of the surficial deposits with a constant elevation of zero.

Eruptive volumes may be estimated once we have the outcrop data and the corresponding elevations. These estimates allowed the inference about chamber volumes. Gross estimates were considered, since the chamber volumes will change in the computational model during the calibration process. Moreover, depending of how the eruptive volumes are calculated, differences of 50% or even more are commonly observed (see for example Brueseke and Hart [22]).

The estimates of eruptive volumes were made by subtracting reference values to the actual elevation in order to obtain an approximate thickness of the deposits. This is because detailed data on thickness of volcanic units are lacking. The subtracted value to the elevation of the LTV volcanic complex was 450 m, this means that the products

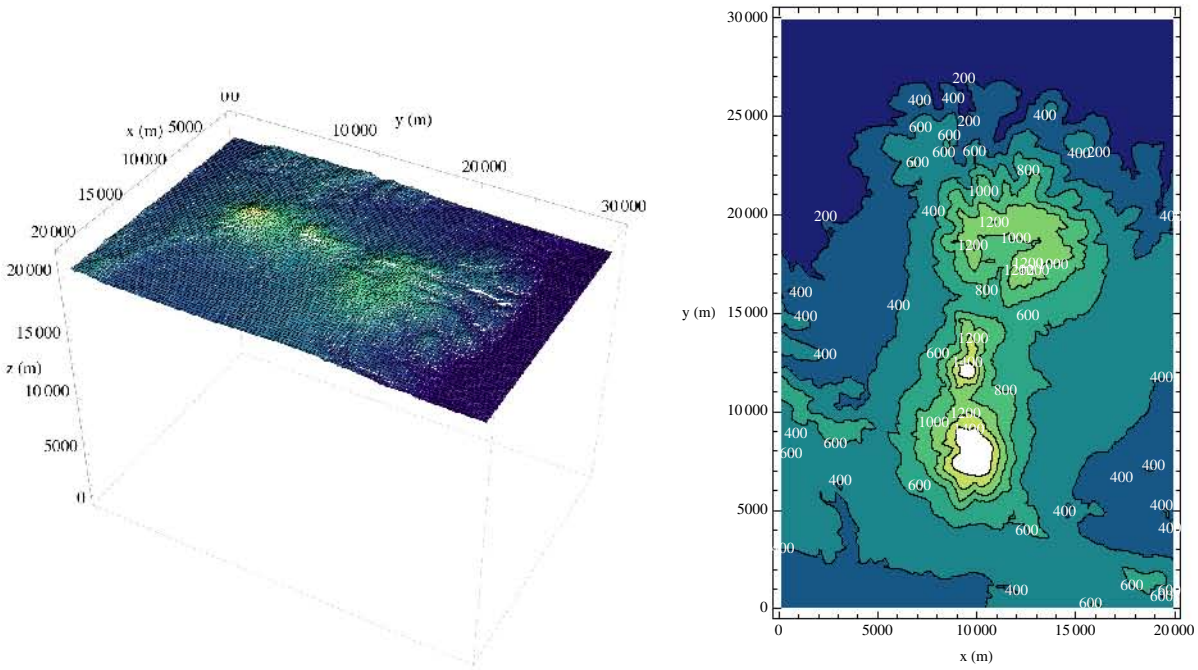

Figure 2.7: Topography of the study area: Three-dimensional view of the discretized topography and the corresponding contour plot. Maximum elevation is related to La Virgen volcano (see Figure 2.3 for reference). Elevation between 600 and 800 m a.s.l. is observed in the geothermal area.

bellow this elevation were not considered as part of the LTV eruptive products. A value of 100 m was subtracted to the Aguajito rhyolitic domes, and 250 m, to remaining Aguajito outcrops. The subtracted values are mean elevations in the limit of the outcrops of the LTV and Aguajito complexes.

The resulting eruptive volumes, EV, of the LTV volcanic complex and Aguajito caldera (AGC) were, respectively:

$$\boxed{EV_{LTV} = 27 \text{ km}^3 \qquad \text{and} \qquad EV_{AGC} = 47 \text{ km}^3}$$

The chamber volumes may be estimated from these values by multiplying by a factor of about 8 [23, 24]. Figure 2.8 shows a schematic representation of the volcanic system with chamber volumes of V_{LTV}=194 km^3 and V_{AGC}=288 km^3 and a depth of the top of both chambers (d_{cham}) of 3000 m b.s.l.. This combination of volumes and depth provided consistent results with the estimated formation temperatures (Chapter 5).

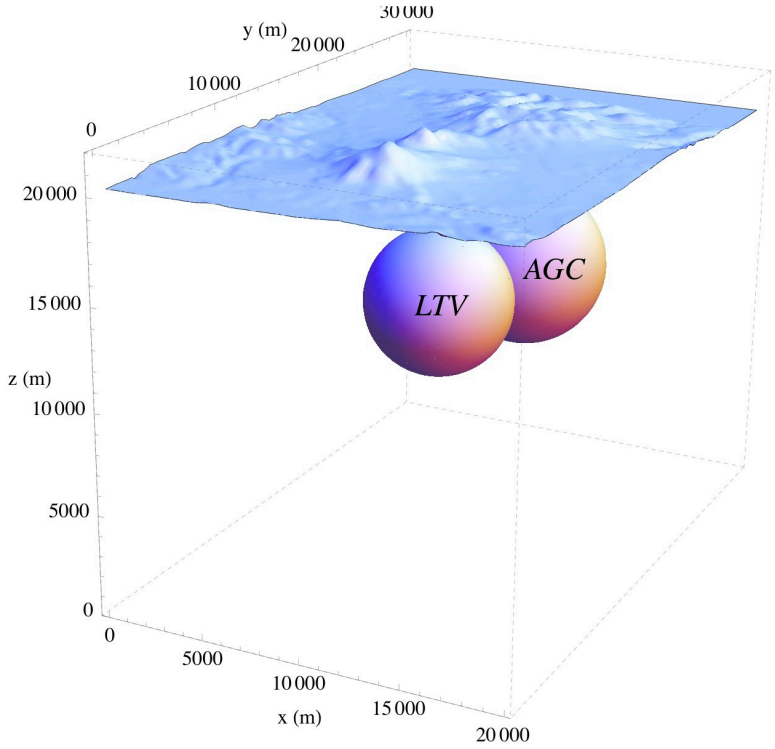

Figure 2.8: Schematic model of LTV volcanic complex. V_{LTV}=194 km^3, V_{AGC}=288 km^3, d_{top}=3000 m b.s.l.. LTV= Las Tres Vírgenes magma camber; AGC= Aguajito Caldera magma chamber.

Finally, the scalar field of thermal diffusivity was defined based on lithologic studies reported in the literature [11, 15, 20, 21] (Table 2.1) and physical properties of the rocks that constitute the main composition of each lithological unit (Table 2.3).

An approximated equation of the fault plane that acted as a barrier for the sedimentary deposition (sediements of Santa Rosalía basin) was calculated from the detailed map of the geothermal zone reported by López-Hernández [15] (Figure 2.9).[2]

The resulting equation of the plane is

$$y = -0.233x + 16790.4 \tag{2.2}$$

Although the equation is independent of z, it is an acceptable approximation since

[2]López-Hernández [15] reports that this fault is named El Viejo, however according with the maps in there, the boundary of the sedimentary unit is the El Partido fault. This fault is considered for calculating the equation.

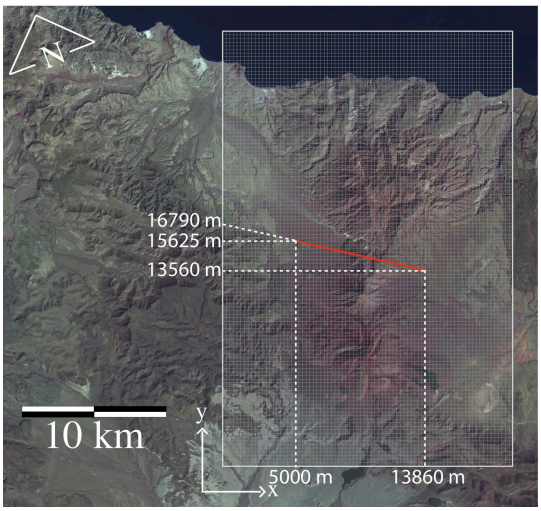

Figure 2.9: Schematic representation of the El Viejo fault (red solid line). This fault is a subsurface boundary of the lithological unit of sediments of Santa Rosalía (from López-Hernández [15]). The equation of the plane (Eq. 2.2) was calculated from the coordinates shown.

the influence of the fault is only in shallow depths. However, it would be important to include more field data for a more accurate discretization of the geothermal area. The resulting distribution of diffusivity is like a composite wall with a lateral variation in the interval $z \in (20367, 20467)$ restricted by the Equation 2.2. The diffusivity field $\alpha(x, y, z)$ was defined as follows:

$$\alpha(x,y,z) = \begin{cases} 9.85 \times 10^{-7}, & \text{if } 0 \leq z \leq 19550,\ \forall x,\ \forall y; \\ 4.85 \times 10^{-7}, & \text{if } 19550 < z \leq 19950,\ \forall x,\ \forall y; \\ 5.10 \times 10^{-7}, & \text{if } 19950 < z \leq 20367,\ \forall x,\ \forall y; \\ 5.10 \times 10^{-7}, & \text{if } 20367 < z \leq 20467,\ (x,y) \mid y \leq -0.233x + 16790.4; \\ 7.0 \times 10^{-7}, & \text{if } 20367 < z \leq 20467,\ (x,y) \mid y > -0.233x + 16790.4; \\ 5.10 \times 10^{-7}, & \text{if } 20467 < z \leq 21923,\ \forall x,\ \forall y; \end{cases} \tag{2.3}$$

Note that lithological units were extrapolated where data are lacking. For example, the granodioritic basement is extrapolated in z direction, $0 \leq z \leq 19550$, and for all x and y ($\forall x$, $\forall y$). Although the diffusivity field is also extrapolated in the atmospheric

Table 2.3: Diffusivity of lithological units of the LTV geothermal field.

Formation	Composition	Thermal Diffusivity (m^2/s)
Basement	Granodioritic	9.85×10^{-7}
Comondú Group	Andesitic	4.85×10^{-7}
Santa Lucía	Andesitic	5.10×10^{-7}
Sediments of Santa Rosalía basin	Sandstone	7.0×10^{-7}
Surficial deposits	Andesitic	5.10×10^{-7}

region, the atmosphere is discarded in the numerical model in order to define a constant temperature boundary condition (Section 4.2).

The definition of $\alpha(x, y, z)$ is certainly simplified. More field data for mapping the lithological units and experimental work for characterizing physical properties of these units would be recommended for refining this conceptual model. Nevertheless, the computational model allows a sensitivity analysis of the physical properties.

Before developing the numerical model of the system, two applications of the computational model THCEMSYS were studied. This provided the experience required to know the intricacies of the magma chamber-reservoir model. These applications are described in Chapter 3.

Chapter 3

Three-dimensional simulation model TCHEMSYS and applications

3.1 Three-dimensional magma chamber-reservoir model

The TCHEMSYS computational model was developed in the Centro de Investigación en Energía of the Universidad Nacional Autónoma de México [8]. It is a three-dimensional (3D) simulation model of thermal-chemical behavior of coupled magma chamber-reservoir system. The model simulates the cooling of a cylindrical magma chamber by conduction and convection, considering process of mineral crystallization, partial assimilation of crust, and magma re-injection. Full details may be found in Verma and Andaverde [8]. Below is a brief summary of the characteristics of the model.

The physical model was defined for a maximum domain of $30000 \times 30000 \times 20000$ m ($x - y - z$ system), in which a cylindrical magma chamber cools conductively and convectively through time (Figure 3.1). The heat transfer equation was discretized by the finite volume method with a uniform mesh of 250 m-edge control volumes. These definitions were made according to the computational facilities available at the moment of the model design, however, a larger domain can be studied today. Finer meshes can also be considered, however, some restrictions are present regarding to the magma chamber processes, as will be described further in this chapter. The physical properties of the

system are set by the user through an input file. In the present version of the TCHEMSYS model, only z-dependence of thermal diffusivity is permitted.

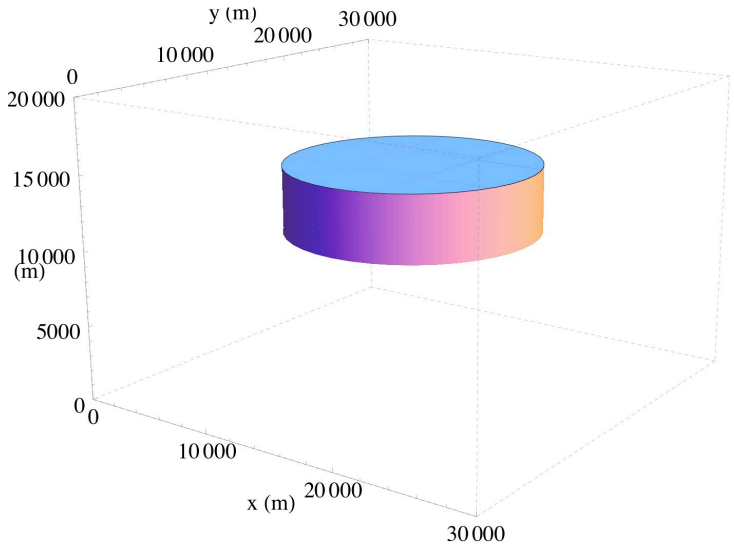

Figure 3.1: Schematic model of TCHEMSYS. V_{cham}=1000 km^3, d_{top}=5000 m, 8500 m of radius. This domain is discretized with control volumes of dimensions $250 \times 250 \times 250$ m, resulting 1152000 blocks.

The program was written in Fortran 90 and consists of eight modules that simulate processes from magma chamber emplacement in module 1 to the formation of the reservoir, in module 8. Modules 2 to 7 are used to compute the thermal-chemical evolution of the system.

The input data needed for the simulation are obtained from geological and geochemical information of the volcanic system studied: dimensions of the domain, physical properties of the layers, initial composition of magma, and chamber volume and depth.

To date the program has been applied to the study of two geothermal fields: the Los Humeros, Puebla, and La Primavera, Jalisco, [9, 10]. All TCHEMSYS modules were applied in the first study due to the availability of a fractional crystallization model of the Los Humeros caldera. The second application, La Primavera caldera, consisted in magma chamber emplacement and thermal evolution modeling without chemical evolution due to the lack of the corresponding fractional crystallization model.

3.2 Application to the La Primavera caldera: geothermometric aspects

The La Primavera caldera constitutes a promising geothermal field with 13 deep wells already drilled. It lies near the triple junction of the Tepic-Zacoalco, Colima and Chapala rifts in the western part of the Mexican Volcanic Belt. The only temperature field simulation study of this caldera in two dimensions is by Verma and Rodríguez-González [25].

Three-dimensional simulation of this geothermal system was developed by the research group responsible of the TCHEMSYS program in the Centro de Investigación en Energía, integrated in 2010 by the authors of the program, an undergraduate and two graduate students (Verma *et al.* [10]). The specific task related with this thesis was the geothermometric analysis of geochemical data for the calibration of the model (see Appendix A for the complete application).

3.2.1 Geological synthesis of La Primavera caldera

The La Primavera caldera is a very young (late Pleistocene), about 12 km diameter, volcanic complex (Figure 3.2). The oldest pre-caldera lavas are about 65 m-thick peralkaline rhyolites at about 400 m depth. The earliest eruptions of pre-caldera lavas took place between about 0.145 and 0.100 Ma. The eruption of the caldera forming event (40 km^3 of Tala tuff) occurred at about 0.095 Ma.

Several eruptive events have been dated using K-Ar method [26]. This dates vary form 0.145 to 0.025 Ma. Drilling has reveled that the oldest units consists of a granitic and granodioritic rocks mainly below about 3000 km subsurface. This deeper layer is overlain by a dominantly andesitic rocks about 1150 m thick. The third lithologic unit about 100 m thick consists of rhyolites. The upper unit is a sequence of lithic tuffs and minor andesites of an average thickness of 750 and 1000 m respectively.

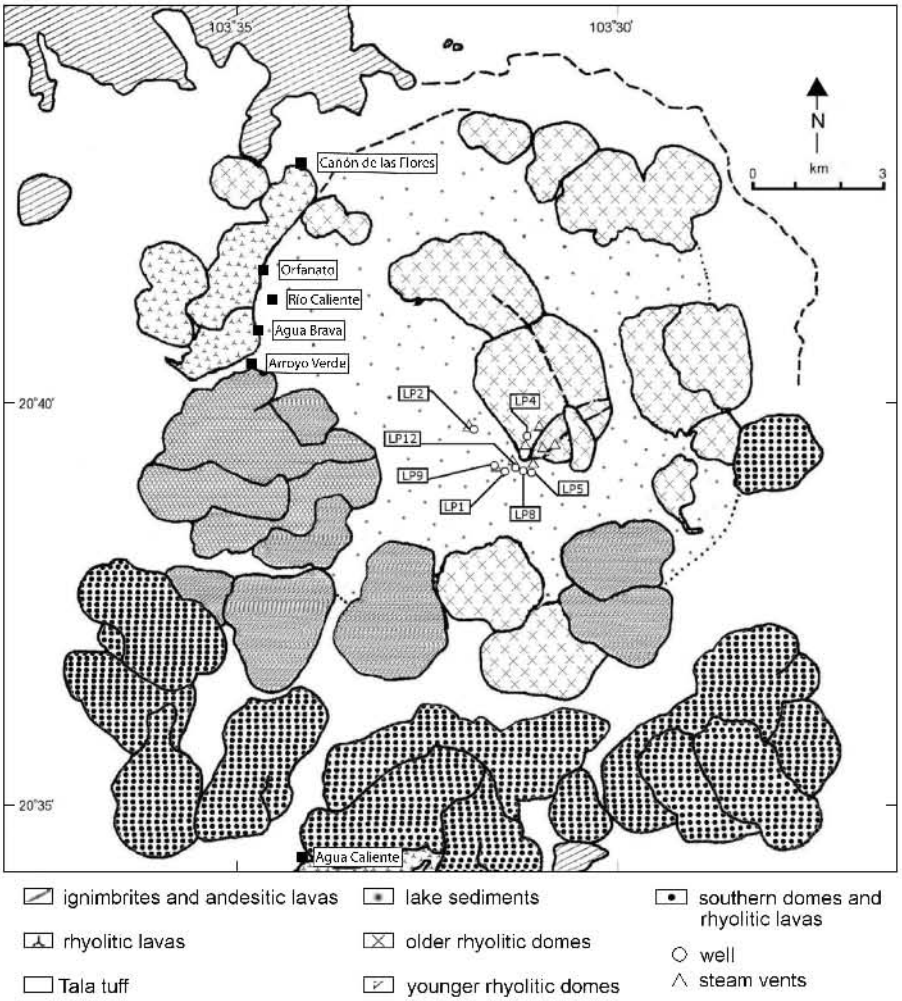

Figure 3.2: Simplified surface geology of the La Primavera caldera, modified after Mahood (1977, 1980, 1981a, 1981b). The wells and hot springs referred to in the text are identified.

3.2.2 Geothermometric analysis

Geothermometric estimates of temperatures from fluids of geothermal wells and hot springs were calculated to compare with simulated temperatures. It was assumed that temperature estimates from well fluids corresponds to the bottom hole temperature of the corresponding well. With respect to hot springs there is not a particular depth of the source but a wide region in the geothermal zone. Temperature estimates from hot springs let us establish an intermediate temperature for shallow depths and confirms the geothermal potential of the area.

Mahood *et al.* [27] and Villa Merlo *et al.* [28] carried out geochemical analysis of water of hot springs and geothermal wells in the La Primavera geothermal field. Their data were used to calculate our gethermometric estimates, Table 3.1 and 3.2.

Table 3.1: Chemical composition of water samples from thermal springs and geothermal wells of the La Primavera geothermal field obtained by Mahood *et al.* [27]. Units: mg/kg.

Locality	T(°C)	Cl	HCO_3	SO_4	Na	K	Li	Ca	Mg	SiO_2
Hot springs										
Orfanato (O)	58	112	452	43	267	11	0.88	5.4	0.81	218
Río Caliente (RC)	67	106	487	43	280	11	0.92	3.5	0.4	227
Agua Brava (AB)	67	94	495	31	268	12.5	0.9	3.8	0.46	207
Arroyo Verde (AV)	68	94	487	30	268	11	0.87	4.1	0.46	215
Agua Caliente (AC)	63	155	377	5	275	9.5	1.05	1.5	0.35	177
Thermal well										
Cañón de las Flores (CF)	35	5.4	90	6	35	2.8	0.04	2.3	0.86	123
Geothermal wells										
LP2 (Nov. 81)	—	1120	2350	234	2000	107	8.5	0.2	0.01	632
LP2 (Mar. 82)	—	1500	3592	362	3310	193	3.9	0.02	0.08	315
LP1 (Oct. 81)	—	851	360	61	650	105	9.9	0.8	0.01	597

Table 3.2: Chemical composition of water samples from geothermal wells of the La Primavera geothermal field obtained by Villa Merlo *et al.* [28]. Units: ppm.

Geothermal Well	HCO_3	Na	K	SiO_2
LP2	2886	2444	130	550
LP9	230	666	148	1202
LP1	426	660	112	877
LP1	140	740	140	1249
LP8	419	824	159	1041
LP5	910	685	54	404
LP5	580	745	117	606
LP5	632	582	70	—
LP5	680	548	48.5	478
LP4	882	440	35.5	227

Temperature estimates were calculated with the computer program SolGeo developed by Verma *et al.* [29]. An improved Na-K geothermometer of Verma and Díaz-González

[30] was also included. Only those geothermometers for which respective errors could be determined were considered (Table 3.3). Minimum and maximum temperature estimates for each sample site are presented in Table 3.4 and in Figure 3.3.

Table 3.3: Solute Geothermometers

Geothermometer	Equation	Reference
Na-K (Fournier)	{1217(±93.9)/[log(Na/K)+1.483)]}-273.15	F79
Na-K (Verma-Santoyo)	{1289(±76)/[log(Na/K)+0.615)]}-273.15	VS97a
Na-K (Díaz-González *et al.*-1)	{883(±15)/[log(Na/K)+0.894(±0.032)]}-273.15	DSR08
Na-K (Verma-Díaz-González)	{868.3(±12.7)/[log(Na/K)+0.8744(±0.0269)]}-273.15	VD11
Na-Li (Fouillac-Michard-1)	{1000(±47)/[log(Na_m /Li_m)+0.38(±0.11)]}-273.15	FM81
Na-Li (Verma-Santoyo-1)	{1049(±44)/[log(Na_m /Li_m)+0.44(±0.10)]}-273.15	VS97b
Quartz (Fournier-Potter)	-42.198(±1.345)+0.28831(±0.01337)S-	
$3.6686\times10^{-4}(\pm3.152\times10^{-5})S^2+3.1665\times10^{-7}(\pm2.421\times10^{-7})S^3$ +77.034(±1.216)log(S)		FP82
Quartz (Verma-Santoyo-2)	[140.82(±0.00)]+[0.23517(±0.00179)]S	VS97c

Na-K F79 and VS97a applicable for temperature>150°C; DSR08 applicable for temperatures between 30 and 350°C; Na-Li FM81 and VS97b for Cl<0.3 mol/kg.

Figure 3.3-A shows consistent results in upper and lower temperatures estimates from hot springs related to Río Caliente fault (O, RC, AB, AV). The lowest temperatures are related to Agua Caliente hot spring, at the southwest margin of the complex, and Cañón de las Flores thermal well, the most diluted sample. This behavior is consistent with the different origin, and equilibrium conditions, of the samples.

As may be observed (Figure 3.3-A), all the intervals are wide, the smallest corresponds to Agua Brava [121(±8)-183(±3)] obtained with VD11 and VS97c, and the largest corresponds to Cañón de las Flores [84(±22)-170(±11)] from FM81 and DSR08. The disagreement between the estimates is related with both the equilibrium condition of the fluids and analytical errors. Processes of conductive cooling and re-equilibration of fluids may be important.

Temperature estimates from geothermal wells are, in general, between 250 and 350 °C (Figure 3.3-B). The largest disagreement is related with well LP2. The smallest estimated

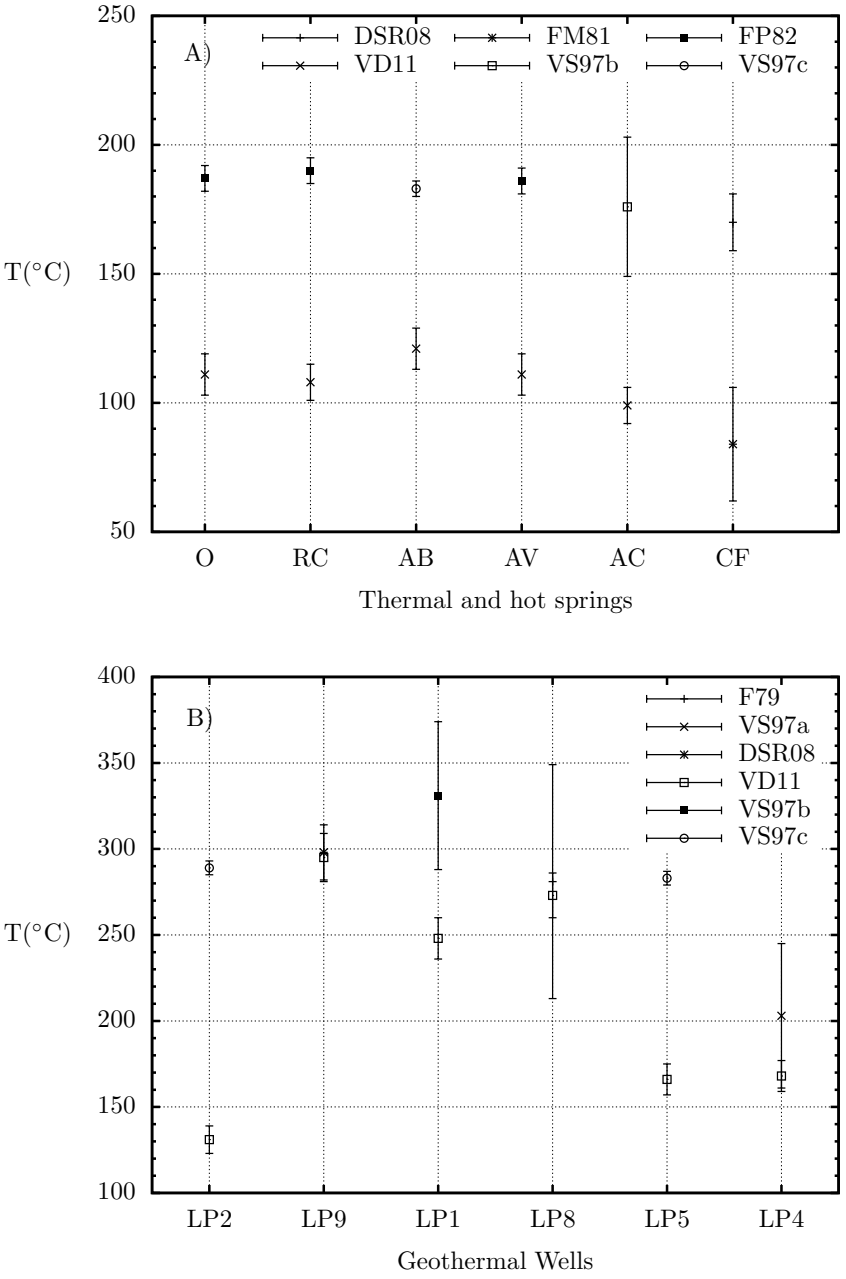

Figure 3.3: Minimum and maximum estimated temperatures from water samples.

temperature for this well was [131(±8), VD11] from both samples LP2 (Nov. 81) (Table 3.1) and LP2 (Table 3.2); the largest temperature estimate for this well was [289(±4), VS97c] from LP2 (Nov. 81) (Table 3.1). In relation to well LP1, the smallest estimate was [248(±12), VD11] form LP1 (Oct. 81) (Table 3.1); the largest estimate corresponds

Table 3.4: Estimated subsurface temperature intervals

Sample	Estimated temperature interval (°C)
Hot springs	
Orfanato (O)	111(±8)-187(±5)
Río Caliente (RC)	108(±7)-190(±5)
Agua Brava (AB)	121(±8)-183(±3)
Arroyo Verde (AV)	111(±8)-186(±5)
Agua Caliente (AC)	99(±7)-176(±27)
Thermal well	
Cañón de las Flores (CF)	84(±22)-170(±11)
Geothermal wells	
LP2	131(±8)-289(±4)
LP9	295(±14)-298(±16)
LP1	248(±12)-331(±43)
LP8	273(±13)-281(±68)
LP5	166(±9)-283(±4)
LP4	168(±9)-203(±42)

to [331(±43), VS97b] from the same sample. The estimates from well LP5 also has a large disagreement; as may be seen in Table 3.2, there are important variations in the composition of this well and more field data would be required for clarifying this behavior.

These temperature intervals along with measured temperatures were used for the model calibration. Table 5 (Appendix A) shows these results. Even the best model (Model D; see conclusions in Appendix A) has important disagreements. This model provides lower bottom hole temperatures than measured temperatures (LP1, LP8, and LP5), which is contrary to the physically expected. One of the sources of this disagreements is the discretization error related to the mesh used in the numerical model. This aspect is studied in the next application (Section 3.3).

3.3 Domain discretization aspects

The TCHEMSYS model was developed with a uniform mesh, 250 m-edge control volumes, acceptable for simulating magma chamber processes. However, the size of this

control volumes makes it difficult to compare the simulated temperatures in the reservoir with estimated formation temperatures. This is because the simulated temperatures are provided in nodes separated by 250 m, and estimated temperatures are obtained from measurements in a wide rage of depths.

3.3.1 Application of a nonuniform mesh

In order to obtain a better comparison between simulated and estimated temperatures it was proposed a nonuniform discretization scheme of the domain that increases the resolution of the mesh in the z-direction of the reservoir (Figure 3.4). Nonuniform discretization constitute a common practice in computational models in heat transfer and fluid dynamics. Abundant information exists in the literature for a variety of numerical methods in Computational Fluid Dynamics, in particular, for the finite volume method used in TCHEMSYS, such as the book by Versteeg and Malalasekera [31].

A mesh dependence study of the simulation results was developed in order to evaluate the nonuniform mesh and justify its use instead of a finer uniform mesh that would require impractical computation time.

Definition of the physical problem

A particular problem was chosen for reference. The conductive cooling of a cylindrical magma chamber of 1000 km^3 volume, 8500 m radius (4406 m of height) and 5000 m of chamber depth referred to the top (Figure 3.1). It is assumed 1350°C of initial temperature of the chamber. The system domain and physical properties correspond to those used by Verma *et al.* [9].

The simulation time was fixed in 0.02 m.y., a large enough time to allow an appreciable cooling of the magma chamber without requiring large computation time. The mathematical problem is as follows.

$$\frac{\partial T}{\partial t} = \alpha(z)\left(\frac{\partial^2 T}{\partial x^2} + \frac{\partial^2 T}{\partial y^2} + \frac{\partial^2 T}{\partial z^2}\right) \tag{3.1}$$

$$x \in [0, 30000], \qquad y \in [0, 30000], \qquad z \in [0, 20000], \qquad t > 0$$

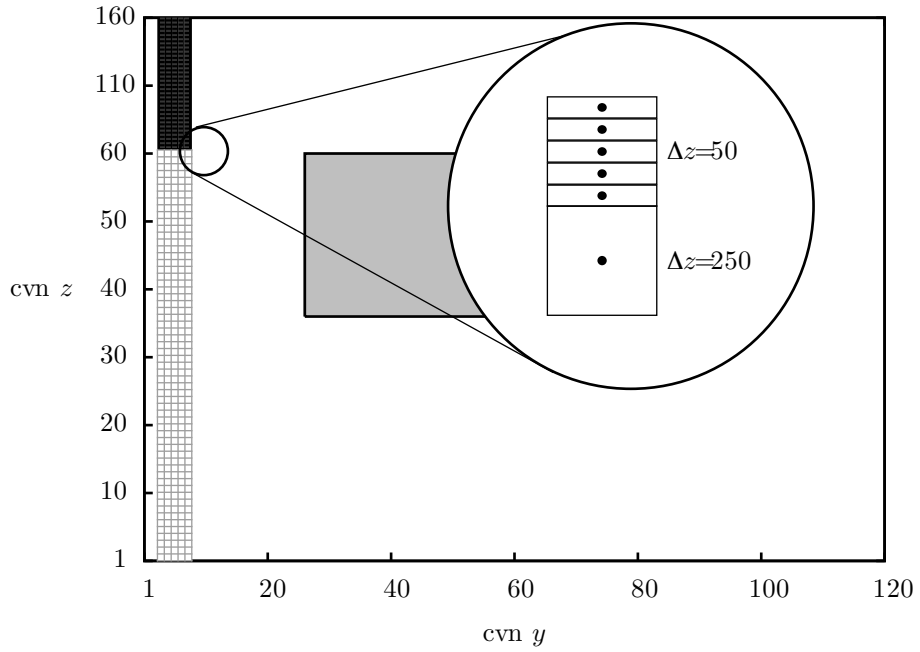

Figure 3.4: Cross section of the TCHEMSYS domain (x=15000 m; Figure 3.1) that shows the number of control volume (cvn) with a nonuniform mesh. This discretization scheme increases the resolution in the reservoir region (above the magma chamber, gray area). Control volumes in y and x directions remain as the default mesh of TCHEMSYS (120 control volumes, Δy=Δx=250 m).

Boundary conditions are set according to the geothermal gradient.

$$T_{geo}(x, y, z) = 25°\text{C} + 0.03\frac{°\text{C}}{\text{m}} \times (20000 - z) \tag{3.2}$$

Initial condition is defined according to the geothermal gradient and 1350 °C in the magma chamber.

$$T(x, y, z, 0) = 1350\ °\text{C} \qquad \text{in the magma chamber (Figure 3.1)}$$

3.3.2 Evaluation of simulation results by means of the norm

A set of nonuniform mesh models was evaluated by comparison of a global parameter of their simulation result with the same parameter of the best solution. The norm of the temperature matrix solution ($\|\mathbf{T}\|$) was chosen as such parameter. A convenient norm is defined in Equation 3.3. This norm may be considered as an approximation to the square

root of the integral of $T^2(x, y, z)$ in the domain and it is only a mathematical expression of the simulation result. The square power of T and the square root are used for generality so that this norm may be applied to any problem in spite of the presence of negative values.

$$\|\mathbf{T}\| = \sqrt{\sum_{i=1}^{nx}\sum_{j=1}^{ny}\sum_{k=1}^{nz}(T^2\Delta V)_{ijk}} \tag{3.3}$$

where

ΔV_{ijk}: volume of the ijk-th control volume;

T^2_{ijk}: square power of temperature in the ijk-th control volume;

nx, ny, and nz: number of control volumes in the corresponding coordinate axis.

The norm of the best solution, of the defined problem, was obtained by means of a convergence analysis of the matrix solution $\mathbf{T}$ for the successively finer uniform meshes. If the numerical method converges to the exact solution when the control volumes tend to a differential size ($nx \to \infty$, $ny \to \infty$, $nz \to \infty$), then the norm $\|\mathbf{T}\|$ will converge to the square root of the integral of $T^2(x, y, z)$ of exact solution. In practical terms, it is not possible to approach closely this value due to computational limitations, round-off errors and solver stability. Nevertheless, it is possible to obtain a good approximation from statistical considerations.

To approximate this norm, 86 successively finer uniform mesh models were simulated according to the following relationships.

$$\begin{aligned} nx_i &= (30 + 3i) \\ ny_i &= (30 + 3i) \\ nz_i &= (20 + 2i) \\ i &= 0, 1, 2, ..., 85 \end{aligned} \tag{3.4}$$

These relationships define the following uniform meshes.

$$\Delta x_i = \frac{30000}{nx_i}$$

$$\Delta y_i = \frac{30000}{ny_i} \tag{3.5}$$

$$\Delta z_i = \frac{20000}{nz_i}$$

$$\Delta x_i = \Delta y_i = \Delta z_i$$

For example, if $i = 0$, the thickest mesh is obtained

$$nx_0 = ny_0 = 30 \qquad nz_0 = 20 \qquad \text{and} \qquad \Delta x_0 = \Delta y_0 = \Delta z_0 = 1000 \text{ (m)}$$

which amounts $nx_0 \times ny_0 \times nz_0 = 18000$ control volumes. If $i = 30$, the original mesh of TCHEMSYS is obtained

$$nx_{30} = ny_{30} = 120 \qquad nz_{30} = 80 \qquad \text{and} \qquad \Delta x_{30} = \Delta y_{30} = \Delta z_{30} = 250 \text{ (m)}$$

which amounts $nx_{30} \times ny_{30} \times nz_{30} = 1152000$ control volumes. The finest mesh is obtained when $i = 85$.

$$nx_{85} = ny_{85} = 285 \qquad nz_{85} = 190 \qquad \text{and} \qquad \Delta x_{85} = \Delta y_{85} = \Delta z_{85} = 105.26 \text{ (m)}$$

which amounts $nx_{85} \times ny_{85} \times nz_{85} = 15432750$ control volumes. Finer meshes were not considered because round-off errors became important.

Time step (Δt) and tolerance (δ)

The Three Diagonal Matrix Algorithm (TDMA) was used iterartively with alternating sweep direction to solve the algebraic system of equations. Eight simulations were carried out in order to evaluate the sensitivity of the results to the tolerance δ used by the iterative application of TDMA (Table 3.5).

A dimensionless computation time (t^*_{cpu}) was defined as the ratio between the total simulation time of a particular model and the total simulation time of the model conventionally used in TCHEMSYS (250 m-edge control volumes, $\Delta t = 0.001$ m.y. and

Table 3.5: Norm ($\|\mathbf{T}\|$) and computation time (t^*_{cpu}) as a function of the tolerance δ for the reference model ($i = 30$, Equation 3.4; $\Delta t = 0.001$).

δ	t^*_{cpu}	$\|\mathbf{T}\|$	δ	t^*_{cpu}	$\|\mathbf{T}\|$
1.0×10^{-3}	0.3	61348	1.0×10^{-7}	1.5	61049
1.0×10^{-4}	0.3	61335	1.0×10^{-8}	2.1	61048
1.0×10^{-5}	0.7	61088	1.0×10^{-9}	2.3	61048
1.0×10^{-6}	1.0	61054	1.0×10^{-10}	2.5	61048

$\delta = 1.0 \times 10^{-6}$) that was about 48 seconds. According to this definition, $t^*_{cpu} = 1.0$ for this reference model.

It is observed a small difference (about 0.01%) between the norm obtained with the reference model and the norm obtained with smaller tolerance. $\delta = 1.0 \times 10^{-8}$, for instance, is recommended since there is no change in the norm for smaller δ, however, t^*_{cpu} is 2.5 times more that that required for the reference model. $\delta = 1.0 \times 10^{-6}$ was considered to provide acceptable results in practical computation time and was used in the remaining simulations.

With respect to Δt, ten simulations were carried out for sensitivity analysis. Five models correspond to 0.02 m.y. of simulation time and five to 0.2 m.y.. In this case, two reference models ($t^*_{cpu} = 1.0$) were defined for each simulation time, both models correspond to the conventional temporal discretization of TCHEMSYS ($\Delta t = 1.0 \times 10^{-3}$ m.y.). The results (Table 3.6) show a small variation of the norm: about 0.03% from $\Delta t = 1.0 \times 10^{-3}$ to $\Delta t = 1.0 \times 10^{-4}$ m.y. for 0.02 m.y. and 0.06% for 0.2 m.y.. Therefore,

Table 3.6: Norm ($\|\mathbf{T}\|$) and computation time (t^*_{cpu}) as a function of Δt (m.y.) for two simulation times: 0.02 m.y. and 0.2 m.y..

	0.02 m.y.		0.2 m.y.	
Δt (m.y.)	t^*_{cpu}	$\|\mathbf{T}\|$	t^*_{cpu}	$\|\mathbf{T}\|$
1.0×10^{-3}	1.0	61054	1.0	56294
5.0×10^{-4}	1.4	61044	1.5	56286
2.5×10^{-4}	2.6	61037	1.9	56277
2.0×10^{-4}	2.8	61039	2.3	56269
1.0×10^{-4}	3.4	61036	4.3	56258

$\Delta t = 1.0 \times 10^{-3}$ provide reliable simulation results for the convergence analysis.

According to these results, it is recommended to consider smaller Δt in models that involve large simulation time since there is a systematic reduction of the norm (temperature) with the reduction of Δt.

Convergence analysis for the mesh size: the norm of the best solution

Considering $\Delta t = 0.001$ m.y. and a tolerance $\delta = 1.0 \times 10^{-6}$, the 86 uniform models (Equation 3.5) were simulated. Figure 3.5 shows the resulting norms. The mean norm was m=60753 with a standard deviation s=325. The largest dispersion is observed before about 500 m-edge control volumes (Figure 3.5). After About 200 m-edge control volumes, norms are confined between 60500 and 61000 without significant reduction of the dispersion from 200 m to the finest mesh (105.26 m-edge).

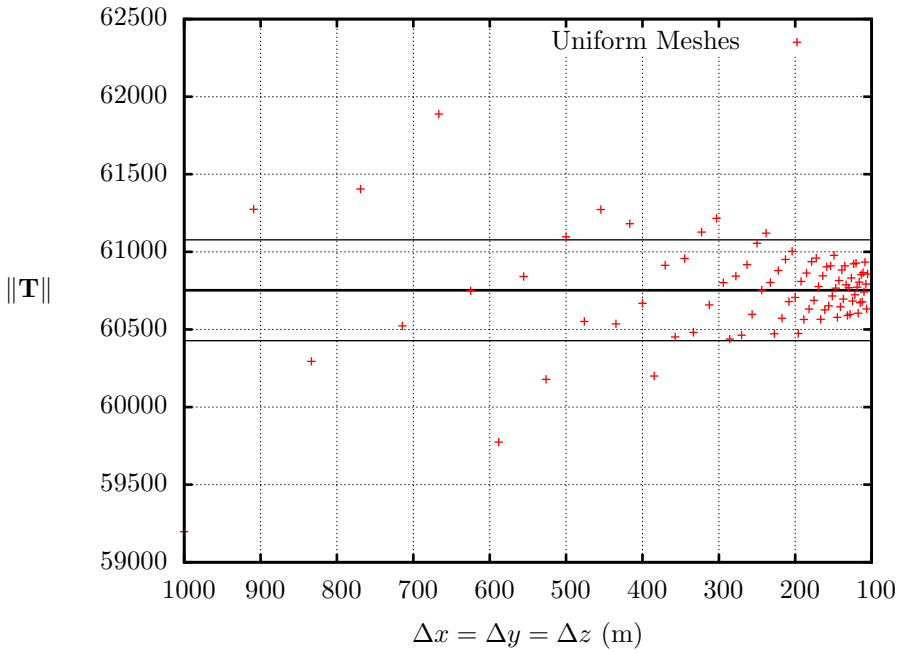

Figure 3.5: Norm of the matrix solution ($\|\mathbf{T}\|$) as the mesh becomes finer. It is observed the expected no linear relation between the increase of control volumes in a coordinate axis (Equations 3.4) and the resulting reduction of the edge of the cubic control volume. No monotone behavior of the series is related to discretization and round-off errors inherent to the computational solution.

Evaluation of the nonuniform mesh models

Six nonuniform meshes were analyzed (Table 3.7) in which different intervals of z axis was refined. Only Δz was varied in these models, this means that Δx=Δy=250 m (nx = $ny = 120$) remain constant as the original mesh of TCHEMSYS. The reduction of Δz has a particular interest since the highest temperature gradients are present in the z direction. As a consequence, better numerical approximations are expected.

Table 3.7: Nonuniform mesh models evaluated (Δx=Δy=250 m for all cases). Model NU-A is illustrated in Figure 3.4.

Reference Name	Δz (m)	z interval†	nz	Number of blocks $nx \times ny \times nz$	t^*_{cpu} ‡	$\|\mathbf{T}\|$
NU-A	50	$(15000, 20000)$	160	2304000	3.2	61030
NU-A2	25	$(15000, 20000)$	260	3744000	5.1	61017
NU-B	50	$(0, 20000)$	400	5760000	8.4	60781
NU-B2	25	$(0, 20000)$	800	11520000	16.6	60820
NU-C	50	$(0, 10500) \cup (15000, 20000)$	328	4723200	6.6	61001
NU-D	50	$(10500, 15000)$	152	2188800	3.5	60796

† Remainder interval of z is divided into 250 m as originally.
‡ t^*_{cpu} is referred as in Table 3.5.

Nonuniform models may be classified in two groups, those in which the z-interval where the chamber is placed ($z \in [10549, 15000]$) is refined (NU-B, NUB-2 and NU-D) and those in which the refined z-interval does not include the chamber (NUA, NU-A2 and NU-C). Figure 3.6 shows the corresponding temperature profiles obtained with these models. It is observed the variable number of nodes –simulated temperatures– for each nonuniform model. Although the temperature profiles are qualitatively similar, there are differences as may be observed in the histogram (Figure 3.7) that shows temperature differences at the same z-values of NU-A and NU-B thermal gradients. Up to 40 °C of temperature difference is observed.

The resulting norms of the nonuniform models (Table 3.7) were compared with the mean norm obtained in the convergence analysis. Figure 3.8 shows this comparison along with the original uniform mesh of TCHEMSYS. As expected, the norms of all nonuniform meshes are closer to the mean value than the original mesh. The closest group to the mean

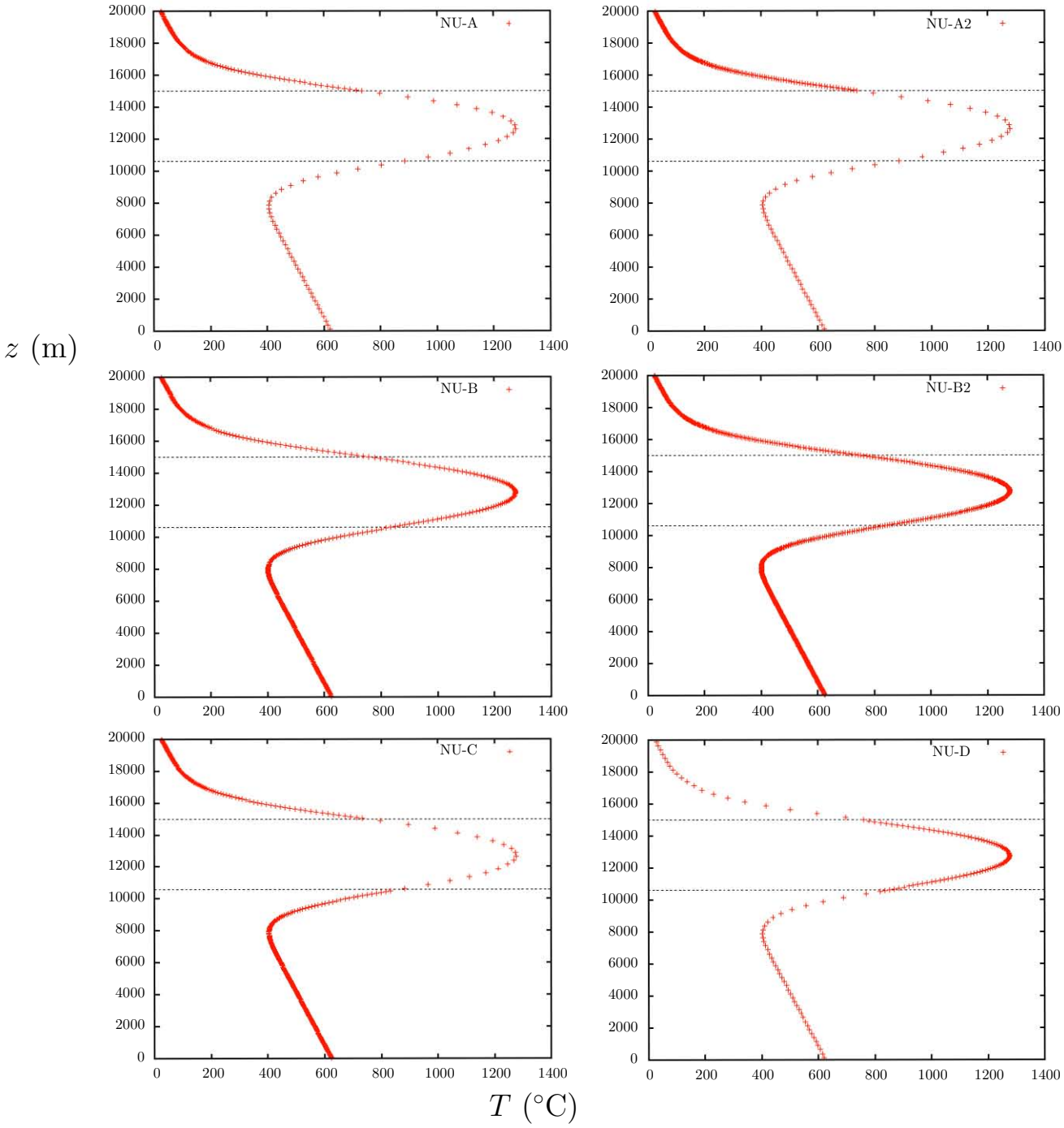

Figure 3.6: Temperature profiles of nonuniform models (Table 3.7) at $x = 15000$, $y = 15000$. The magma chamber is schematically shown by dotted lines. It is observed the variable number of simulated temperatures in the z-direction according to each model. ΔT in equal z-values of the models NU-A and NU-B is shown in Figure 3.7.

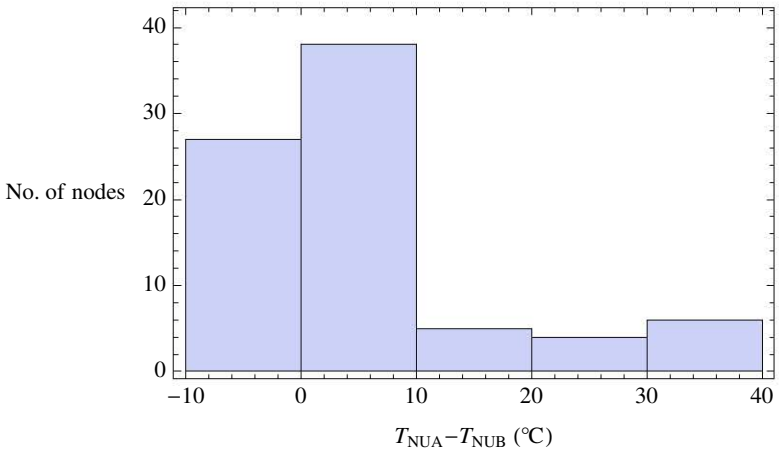

Figure 3.7: Histogram of temperature difference of NU-A and NU-B gradients (Figure 3.6). The temperature difference was made in coincident z-values of 80 nodes 250 m-equally spaced.

norm (NU-B, NU-B2 and NU-C) consists of the models that refine the z-interval where the chamber is placed, improving the approximation of the heat flux in a high gradient region. Therefore, these nonuniform schemes are recommended. A slight improvement may be observed in the models NU-A, NU-A2 and NU-C with a finer mesh out of the chamber. Besides, their do not require too much consumption of computational resources.

The closest norm to the mean value corresponds to model NU-B in which the complete z axis was divided into 400 (Δz=50 m; Table 3.7). The model NU-B2 (Δz=25 m in all z axis) provides a slightly larger norm than NU-B. This increase is related to the no monotone behavior of the series. As may be confirmed in the convergence analysis (Figure 3.5), even the norm of the finest uniform meshes present dispersion because of discretization and round-off errors. As a consequence, no important improvement of the result is expected from reducing Δz=50 m to smaller values.

Before selecting an appropriate mesh for the TCHEMSYS model, it is necessary to consider some restrictions. From chamber emplacement to velocity distribution in magma and fractional crystallization, these processes are modeled to occur in a uniform mesh (Δx=Δy=Δz) in the chamber region. The emplacement of the chamber was modeled by a gradual magma input of 250 m-thick discs with a defined radius. Therefore, a

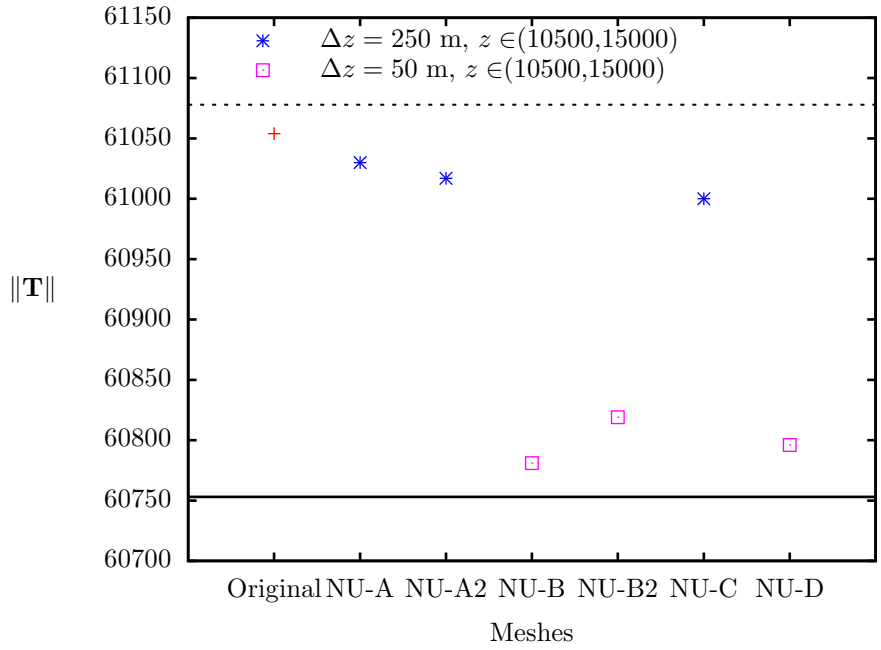

Figure 3.8: Evaluation of the nonuniform discretization schemes by comparison with the mean norm (solid line) and standard deviation (dotted line) obtained in the convergence analysis (Figure 3.5). Nonuniform models are classified according to whether they refine the z-interval where the chamber is placed. Original TCHEMSYS uniform mesh is included for comparison.

nonuniform mesh that involves the chamber, in addition to the upper layers, would require a new emplacement scheme. In relation to velocity distribution and mass transport, major changes in the program structure would also be necessary. Therefore, the discretization schemes permitted by TCHEMSYS in its present version are NU-A, NU-A2 and NU-C.

The mesh analysis developed here may be extended to the problem with gradual emplacement and convection. Convective heat transfer only improves the heat flux from the chamber to the surroundings, but initial and boundary conditions are the same. Considering that the conductive and convective terms in the TCHEMSYS model are of the first order, the accuracy improvement provided by the nonuniform schemes is likely to be similar in both conductive and convective problems.

Chapter 4

Numerical model for the Las Tres Vírgenes geothermal field

4.1 Domain discretization

Once the conceptual model of the LTV geothermal field was defined (Chapter 2) and discretization aspects were studied (Chapter 3) the numerical model was proposed. The more detailed conceptualization of the system and the application of nonuniform mesh produced a better coupling of the magma chamber-reservoir system.

The equation to solve is the heat equation:

$$\frac{\partial T}{\partial t} = \alpha(x,y,z)\left(\frac{\partial^2 T}{\partial x^2} + \frac{\partial^2 T}{\partial y^2} + \frac{\partial^2 T}{\partial z^2}\right) \tag{4.1}$$

$$x \in [0, 30000], \qquad y \in [0, 30000], \qquad z \in [0, 21923], \qquad t > 0$$

where $\alpha(x,y,z)$ is the thermal diffusivity defined in Section 2.4.1 (Equation 2.3).

The initial condition is given by the geothermal gradient and the beginning of the emplacement of Aguajito chamber. The boundaries are maintained at the temperature of the geothermal gradient. These aspects will be analyzed in Section 4.2.

In the conceptual model, x-domain was defined as $x \in [0, 20000]$ m (Section 2.4). However, in the numerical model additional 10000 m were included in the x axis in order to reduce the influence of the boundaries on the conductive cooling. This is because a

constant temperature (geothermal gradient) is assumed away from the chambers. Physical properties and topographic data were extrapolated in this additional domain (x-direction) since the purpose is only to move away the boundaries. Note that the resulting numerical domain is almost equivalent to the TCHEMSYS domain ($30000 \times 30000 \times 20000$ m; $x-y-z$ system), with a difference in the z-axis due to the inclusion of the topography.

Considering the good performance of the Finite Volume method in the model THCEMSYS [8], this method was used to develop the LTV computational model. The details of the discretization may be found in many books on the subject. Results of the discretization are presented here using the notation of Versteeg and Malalasekera [31].

The discretization of the heat equation (Equation 4.1) in a no-boundary control volume P (Figure 4.1-A) with a fully implicit scheme for approximating the time dependence produces a heptadiagonal linear system given by

$$a_P T_P = a_E T_E + a_W T_W + a_N T_N + a_S T_S + a_T T_T + a_B T_B + s_P \tag{4.2}$$

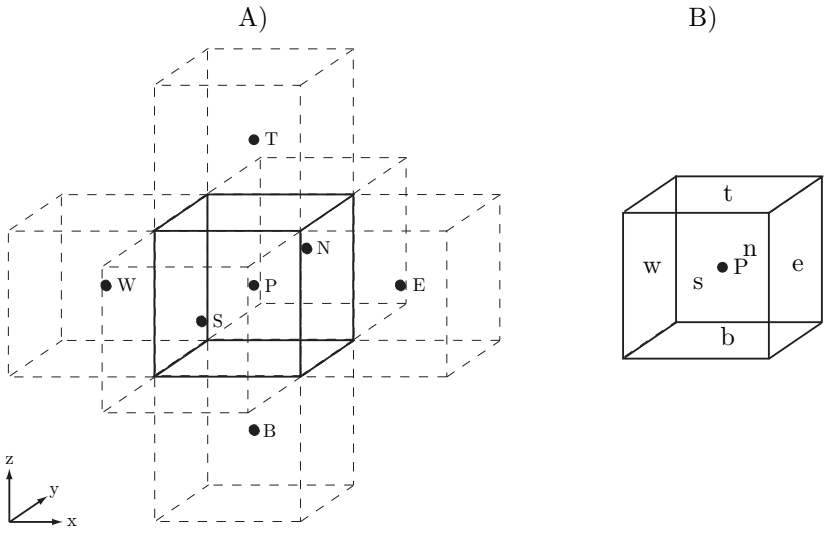

Figure 4.1: Control volume of the three dimensional system. A) The neighbors of the control volume P are labeled in capitals according to the directions north, south, east, west, top, and bottom. B) Lowercases, of the same directions, are used to label the faces of the control volume.

with

$$a_E = \frac{\alpha_e s_e}{\Delta x_{PE}}, \quad a_W = \frac{\alpha_w s_w}{\Delta x_{WP}}, \quad a_N = \frac{\alpha_n s_n}{\Delta y_{PN}}$$
$$a_S = \frac{\alpha_s s_s}{\Delta y_{SP}}, \quad a_T = \frac{\alpha_t s_t}{\Delta z_{PT}}, \quad a_B = \frac{\alpha_b s_b}{\Delta z_{BP}} \tag{4.3}$$

All variables and parameters are calculated either in the centers -nodes- (capital subscripts) or in the faces (lowercase subscripts) of the control volumes (Figure 4.1-A and Figure 4.1-B, respectively).

Δx_{PE} is the distance between the nodes P and E. The remainder deltas are defined analogously.

α_e, α_w, ..., α_b are the diffusivities in the corresponding faces of the control volume (Figure 4.1-B), they are approximated as follows.

$$\alpha_e = \frac{\alpha_E + \alpha_P}{2}, \quad \alpha_w = \frac{\alpha_W + \alpha_P}{2}, \quad \alpha_n = \frac{\alpha_N + \alpha_P}{2}$$
$$\alpha_s = \frac{\alpha_S + \alpha_P}{2}, \quad \alpha_t = \frac{\alpha_T + \alpha_P}{2}, \quad \alpha_b = \frac{\alpha_B + \alpha_P}{2} \tag{4.4}$$

$s_e, s_w, ..., s_b$ are the areas of the corresponding faces of the control volume P.

The coefficient a_P and the independent term s_P are as follows.

$$a_P = a_E + a_W + a_N + a_S + a_T + a_B + \frac{\Delta v}{\Delta t} \tag{4.5}$$

$$s_P = \frac{\Delta v}{\Delta t} T_P^0 \tag{4.6}$$

where

$\Delta v = \Delta x \times \Delta y \times \Delta z$ $\quad$ T_P^0 : temperature in the node P at the previous time step.

If a boundary temperature is known (Dirichlet condition), the independent term s_P (Equation 4.2) is increased by a quantity depending on what temperature or temperatures are known. If, for instance, the east boundary of the system has a known temperature ($T_{boundary} = T_e = T_E$; Figure 4.2) the independent term of the Equation 4.2 would be $s_p + a_E T_{boundary}$. Besides, the coefficient a_E is modified according to the following consideration. The distance between the node P and the face e (Δx_{Pe}) is equal to $\Delta x_{PE}/2$,

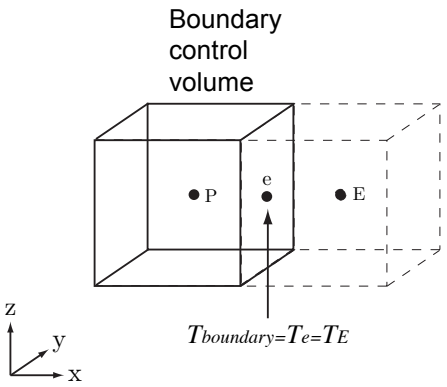

Figure 4.2: Boundary control volume with a known temperature condition $T_{boundary} = T_e = T_E$. Dashed control volume is placed for reference. Note that $\Delta x_{Pe} = \Delta x_{PE}/2$.

therefore the coefficient a_E results as follows.

$$a_E = \frac{\alpha_e s_e}{\Delta x_{Pe}} = \frac{2\alpha_e s_e}{\Delta x_{PE}} \qquad \text{when } T_e = T_{boundary} \tag{4.7}$$

As a consequence, the linear equation for this boundary control volume is as follows.

$$a_P T_P = a_W T_W + a_N T_N + a_S T_S + a_T T_T + a_B T_B + s'_P \tag{4.8}$$

with

$$s'_P = s_P + a_E T_{boundary}$$

and

$$a_E = \frac{2\alpha_e s_e}{\Delta x_{PE}}$$

and the remaining coefficients are calculated as conventionally.

The mesh selected for the LTV numerical model was defined as follows.

$$\Delta x = \Delta y = 250 \text{ m} \qquad \text{and} \qquad \Delta z = 50 \text{ m}$$

This mesh consists of 6307200 control volumes for the domain defined in Equation 4.1. This selection was based on the results with the model NU-B studied in Section 3.3. This mesh is convenient for improving the approximation of the heat flux in the direction of the largest gradients (z-axis) and provides sufficient nodes in the reservoir for a better comparison between simulated temperatures and estimated formation temperatures.

As a first approximation to the best model, the time step was chosen as follows.

$$\Delta t = 1.0 \times 10^{-3} \text{ m.y.} \qquad t \in [0, 0.7]$$

which amounts 700 time steps. Further simulations were made with a time step

$$\Delta t = 1.0 \times 10^{-4} \text{ m.y.} \qquad t \in [0, 0.7]$$

for checking previous results, which amounts 7000 time steps. The iterative application of TDMA method with alternating sweep direction was also used in this model to solve the algebraic system of equations.

4.2 Initial and boundary conditions

The initial condition of the system is defined by the geothermal gradient as well as the beginning of the emplacement of the Aguajito magma chamber (Figure 4.3). The geothermal gradient is defined as 0.03°C/km with a constant surface temperature of 25°C. It is assumed that the geothermal gradient prevails away from the chambers. As a consequence, the temperature is known at the boundaries (Dirichlet conditions).

It is necessary to take into account the topography for the distribution of temperatures in shallow depths. Its effect in the reservoir may be important. Because the initial topography is unknown, elevation of zero was considered. The elevation was modeled to grow gradually until its present state after 0.03 Ma (Equation 2.1), the age of the last eruption. Considering that the sea level corresponds to $z = 20000$ m, the initial geothermal gradient is given by

$$T_{geo}(x, y, z) = 25°\text{C} + 0.03\frac{°\text{C}}{\text{m}} \times (20000 - z) \qquad z \in [0, 20000]$$

Initially, all the region $20000 < z < 21923$ is kept at 25°C since this region has the function of a Dirichlet boundary condition and will host the topography as it grows. Therefore,

$$T(x, y, z) = 25°\text{C} \qquad z \in [20000, 21923]$$

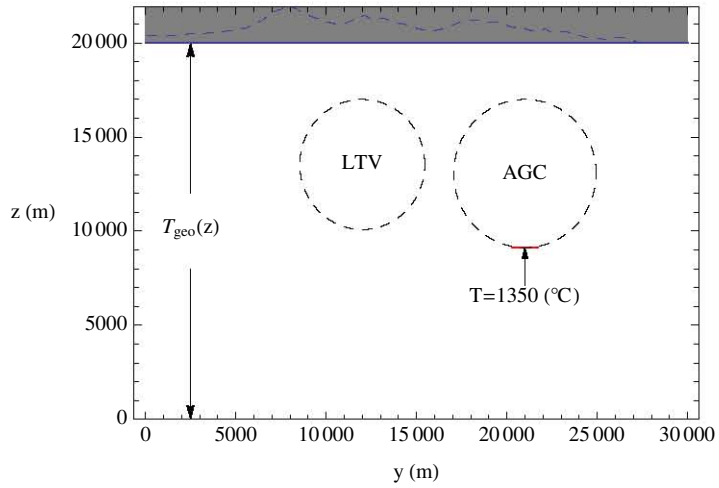

Figure 4.3: Cross section ($x = 10000$ m; Figure 2.8) illustrating the initial condition of the the problem. Shaded area hosts the topographic control volumes as the elevation grows. Initially, this region acts as a boundary with known temperature (surface temperature; 25°C). Dashed circles define the region where the chambers will be emplaced (The Aguajito Caldera chamber=AGC, Las Tres Vírgenes volcanic complex=LTV). The Aguajito chamber starts its emplacement from the bottom at $t = 0$ (Section 4.3).

The growth of the elevation implies that boundary control volumes on the surface have a variable number of constant temperature neighbors. Figure 4.4 illustrates this situation in two dimensions. In Figure 4.4-A the control volumes α and β have only one constant temperature neighbor, nodes 1 and 2, respectively (the discretization is made as conventionally). Figure 4.4-B shows more control volumes that have been activated to take account of the topographic growth. The control volume α' has two constant temperature neighbors (1 and 2) while the control volume β' has three (2, 3 and 4).

From the considerations of the boundary conditions exposed in last section (Section 4.1; Equation 4.8), the discretization in the control volume β' is as follows.

$$a_P T_P = a_S T_S + s_P + (a_E + a_W + a_N) * T_{boundary}$$

where

$$a_P = a_E + a_W + a_N + a_S + \frac{\Delta v}{\Delta t} \qquad s_P = T_P^0 \frac{\Delta v}{\Delta t}$$

and

$$a_E = \frac{2\alpha_e s_e}{\Delta x_{PE}} \qquad a_W = \frac{2\alpha_w s_w}{\Delta x_{WP}} \qquad a_N = \frac{2\alpha_n s_n}{\Delta x_{PN}} \qquad a_S = \frac{\alpha_s s_s}{\Delta x_{SP}}$$

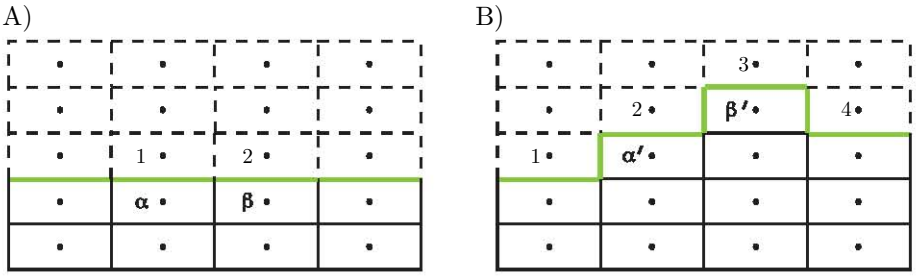

Figure 4.4: Topographic control volumes. Green line represents the topographic boundary, which temperature is known ($T_{boundary}$). Dashed control volumes corresponding to the atmosphere are kept at the boundary temperature, $T_{boundary}$. A) Initial topography; the nodes α and β have only one constant temperature neighbor (north nodes 1 and 2). B) Boundary of topographic growth; the nodes α' and β' have more than one constant temperature neighbor, α' has 1 and 2; β', 2, 3, and 4.

The equations are already solved in constant temperature control volumes (Figure 4.4), since they have the boundary temperature by definition. The equations in these control volumes are as follows.

$$a_P T_P = s_P$$

with

$$a_P = \frac{\Delta v}{\Delta t} \qquad s_P = \frac{\Delta v}{\Delta t} T_P^0$$

hence

$$\frac{\Delta v}{\Delta t} T_P = \frac{\Delta v}{\Delta t} T_P^0 \qquad T_P = T_P^0$$

the temperature is constant in all of these control volumes as long as they are not activated by the topographic growth.

4.3 Emplacement of chambers

Several chamber depths and volumes were evaluated. The (x, y)-coordinates for the chambers (11000,21000) for the Aguajito chamber and (10500,12000) for the LTV chamber led to the best model (see Figure 2.8 for reference).

The emplacement of the chambers was simulated by heating of discs in the granodioritic medium where the chambers were placed (Figure 4.5). The temperature of

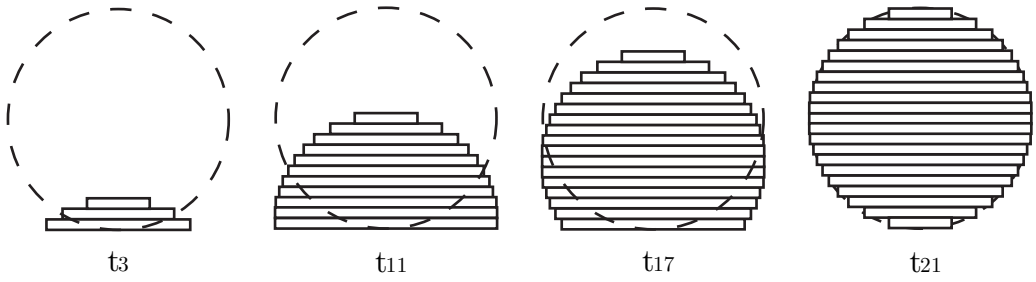

Figure 4.5: Two-dimensional representation of a spherical chamber emplacement by heating and ascending discs. Four no consecutive time steps are presented. Variable radius discs, with a constant thickness Δz, are placed every thousand years ($\Delta t = 0.001$ m.y.) at the bottom of the chamber with a temperature of 1350 °C. The discs are elevated and reheated before a new layer is placed at the bottom until filling the chamber (t_{21}).

emplacement was assumed to be 1350 °C as done before in the TCHEMSYS model, this temperature corresponds to about basaltic magma [32]. Each disc may be considered as a fraction of all the magma chamber that emplaces each time step until the chamber is filled.

The heating of discs is made from bottom to top simulating the process of ascent of magma (Figure 4.5). This emplacement scheme is based on the assumption that opening space in crust is necessary for the emplacement. This assumption requires that the input of magma increases with time, after crustal assimilation have occurred. The spherical geometry chosen allows this variable input of mass to the system since the discs that fill the sphere have variable radius, unlike the constant radius of a cylindrical chamber used in the TCHEMSYS model.

According to magma emplacement processes [33], the upper layers of the chamber crystalize and sink into the magma bellow because they cool faster than the lower layers. This produces an ascent of a new high temperature layer in a cyclic process. In order to take account of this simplified model, a reheat of discs was considered during their ascent. Moreover, because chemical processes in the cambers were not considered, it was necessary to take into account the latent heat of crystallization by reheating the discs during the emplacement. The reheat of the medium is a provisional way to maintain the

energy of the system until a proper chemical analysis of the fractional crystallization and assimilation processes could be achieved.

Chapter 5

Numerical Results

Once the numerical model was defined, a program was written in Fortran 90 that requires an input file for the topography of the geographic area. The computation process was carried out in a unix based operative system. The RAM memory consumption for the process was about 400 Mb.

All the results are presented using the reference system defined in the conceptual model (Section 2.4; Figure 2.8). Fifteen models were analyzed that resulted from combining three depths with five chamber volumes. The models are described in Table 5.1. Both chambers were assumed to be emplaced with its top at the same depth (Figure 4.3).

A dimensionless simulation time (t^*_{cpu}) was defined taking as reference a preliminary model for which $\Delta t = 1.0 \times 10^{-3}$ m.y. and $\delta = 1.0 \times 10^{-6}$ (the mesh was invariable in all these simulations; Section 4.1). 1.5 h were required for the process using these simulation parameters, therefore t^*_{cpu}= Simulation time of a particular model/1.5 h. Further simulations of selected models were carried out using $\Delta t = 1.0 \times 10^{-4}$ and $\delta = 1.0 \times 10^{-7}$.

Model LTV-1.3 (Table 5.1; $\Delta t = 1.0 \times 10^{-4}$ and $\delta = 1.0 \times 10^{-7}$) provided the best agreement with the static formation temperatures (Section 5.3). This model is used to illustrate numerical results in this Chapter.

Table 5.1: Depth of the chambers top (d_{cham}) and chamber volumes (V_{cham}) of 15 models evaluated.

Model	d_{cham}	V_{cham} (km^3)			Re-injected volume
	(m) b.s.l.	Aguajito	LTV	Total	LTV chamber (km^3)
LTV-1.1	3000	320	216	536	40
LTV-1.2	3000	304	205	509	39
LTV-1.3	3000	288	194	482	38
LTV-1.4	3000	272	183	455	36
LTV-1.5	3000	256	173	429	33
LTV-2.1	3500	320	216	536	40
LTV-2.2	3500	304	205	509	39
LTV-2.3	3500	288	194	482	38
LTV-2.4	3500	272	183	455	36
LTV-2.5	3500	256	173	429	33
LTV-3.1	4000	320	216	536	40
LTV-3.2	4000	304	205	509	39
LTV-3.3	4000	288	194	482	38
LTV-3.4	4000	272	183	455	36
LTV-3.5	4000	256	173	429	33

5.1 Emplacement and cooling of magma chambers

Figure 5.1 shows the evolution of emplacement and cooling of the chambers. The topographic growth is observed as the time increases. A small thermal gradient into the cambers is observed, see for instance the LTV chamber at 0.3 Ma (Figure 5.1), where a large high temperature isotherm is shown (1200 °C). This is due to the reheat of the layers as they ascent (Section 4.3). The thermal effect of a re-injection process in LTV volcanic complex is shown in Figure 5.2. In the best models, this process was assumed to occur between 0.08 and 0.062 Ma.

A thermal remnant of the Aguajito chamber is observed. At 0.2 Ma (Figure 5.1), for example, the isotherms (particularly 600 °C) are elongated towards the Aguajito chamber. This thermal remnant is important for the thermal evolution of the system from the emplacement of the LTV magma chamber until the present (present, Figure 5.1).

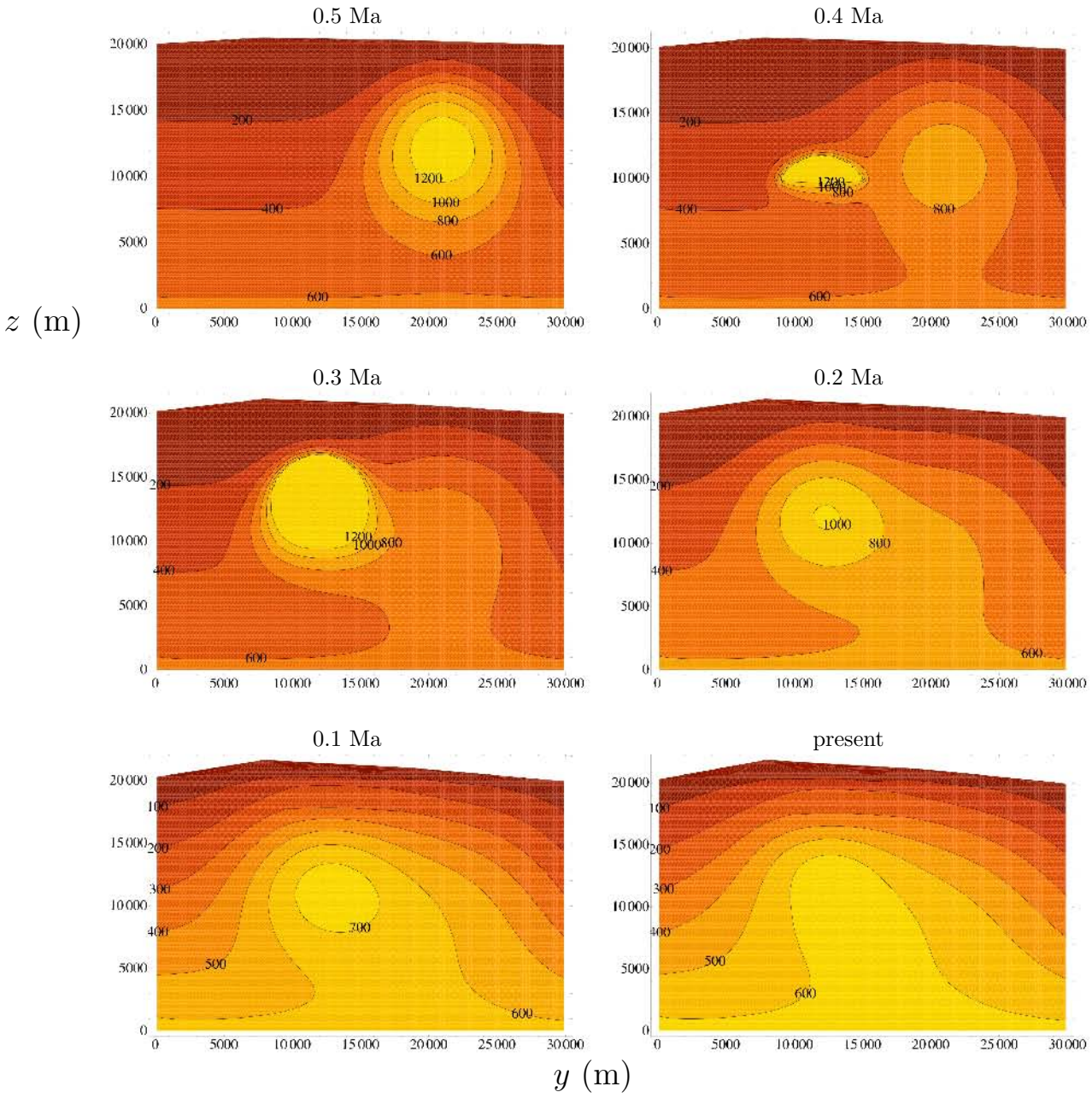

Figure 5.1: Isotherms (°C) in the plane $x = 10000$ (see Figure 2.8 for reference) during emplacement and cooling of chambers. Small thermal gradient in the LTV chamber (y=12000, z=13545 m) is observed during the emplacement due to the reheat of the layers. Thermal remnant of the Aguajito chamber (y=21000, z=13061 m) is clearly observed (0.1 Ma and present) by the elongation of the isotherms towards the Aguajito chamber.

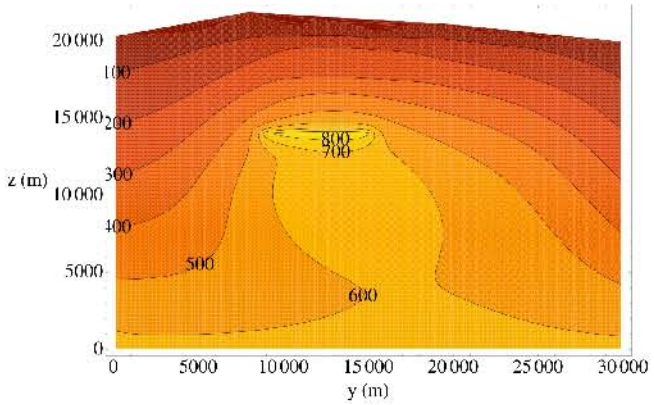

Figure 5.2: 0.07 Ma: Effect of the re-injection process in LTV volcanic complex.

5.2 Temperature field in the geothermal area

The thermal history in the geothermal area referred to the bottom of selected wells (Table 5.1) is presented in Figure 5.3. No important thermal effect occurs in the geothermal area during the emplacement of the Aguajito chamber (0-0.158 m.y.), temperatures of all the wells are lower than 100 °C. During this period, the site of well LV1 shows the largest increase of temperature due to its proximity to the Aguajito complex (drilling sites are shown in Figure 2.2). The largest increase of temperature occurs at the end of the LTV emplacement. Wells LV3 and LV4 are the most sensitive to the conductive cooling due to their location with respect to the chamber.

A change in the thermal evolution is observed at 0.5 m.y. (in particular BHT-LV3, Figure 5.3), this is due to the increase of the heat flux induced by the increase of the conductivity below the reservoir area.

Figure 5.4 shows isotherms in planes (x, y) at three different depths corresponding to the depth of three selected wells. In the case of well LV3, a circular shape around the geothermal area is observed (240 °C), this is due to the selective circular-shaped increase of conductivity that was used. All this area is exposed to a higher heat flux from bellow.

A larger influence of the topography is observed in the temperatures in shallow depths (LV7 and LV8; Figure 5.4). This confirms the necessity of including the topography in the model.

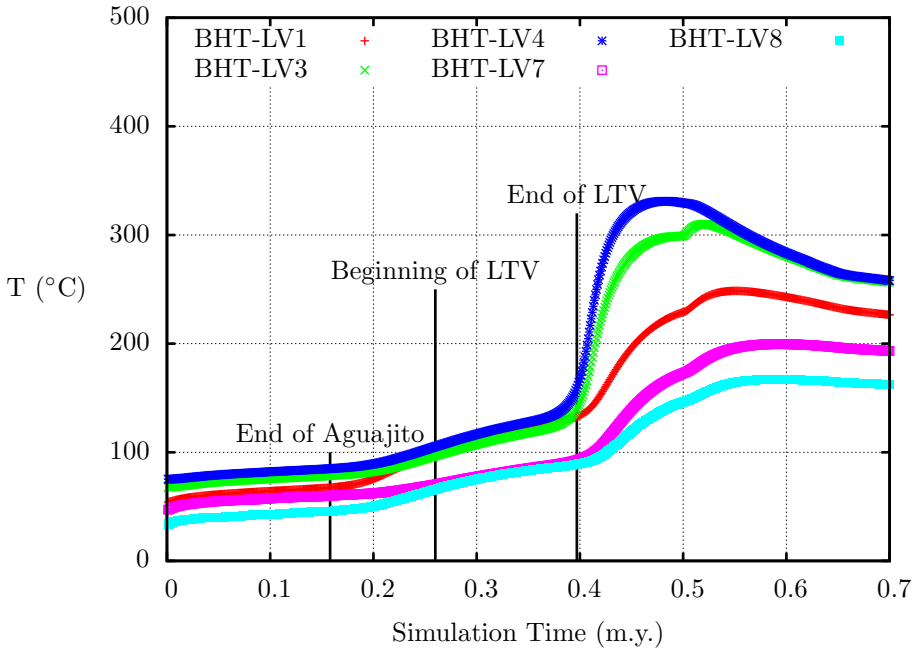

Figure 5.3: Thermal history in the geothermal area obtained with the model LTV-1.3 (Table 5.1). Temperatures are referred to the bottom of the wells (vertical depth; Table 5.2). Periods of chambers emplacement are shown. The largest increase of temperature is observed at the end of the chamber emplacement. Major thermal influence of the LTV chamber for the geothermal area is confirmed.

Figure 5.5 shows the geothermal gradient dependence to the total volume of the chambers. An increase in chambers volume implies an increase of the BHT. This is in contradiction with the results of the TCHEMSYS model [9]. The explanation is related to the different emplacement schemes used. In the TCHEMSYS model, the emplacement is made from the middle part of the chamber to the extremes.

The geothermal gradient referred to well LV3 is shown in Figure 5.6. A high conductivity zone is observed beneath the bottom of well that represents the convective zone for the reservoir. Maximum temperatures are about 650 °C where the chambers are placed.

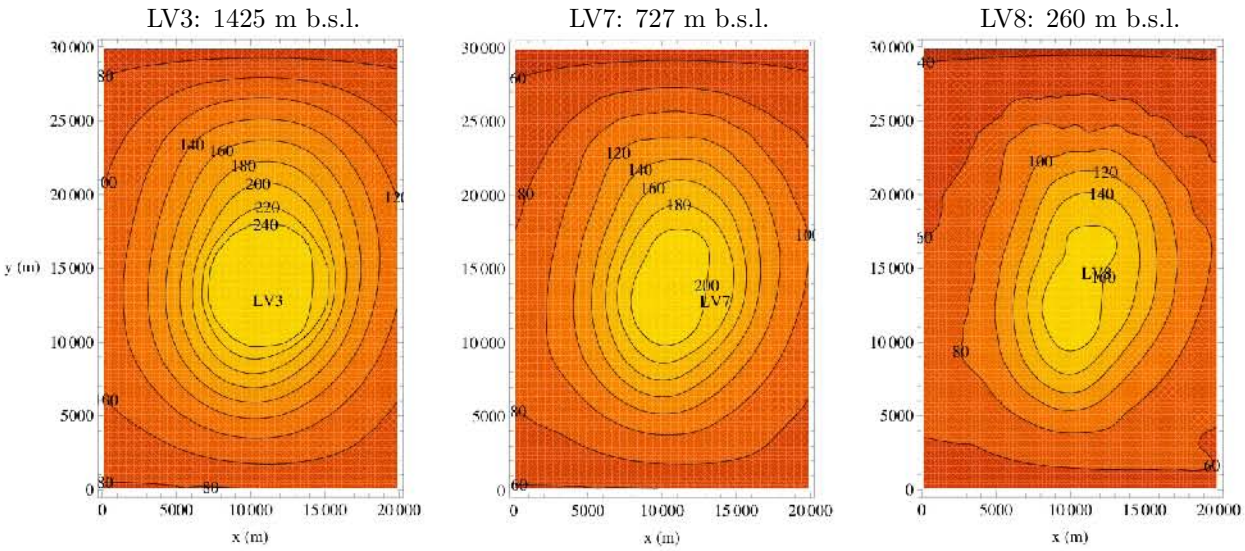

Figure 5.4: Isotherms referred to the depth of wells LV3, LV7 and LV8. Location of the wells is indicated. The influence of the topography is clearly shown in shallow wells (LV7 and LV8; see Figure 2.7 for comparison)

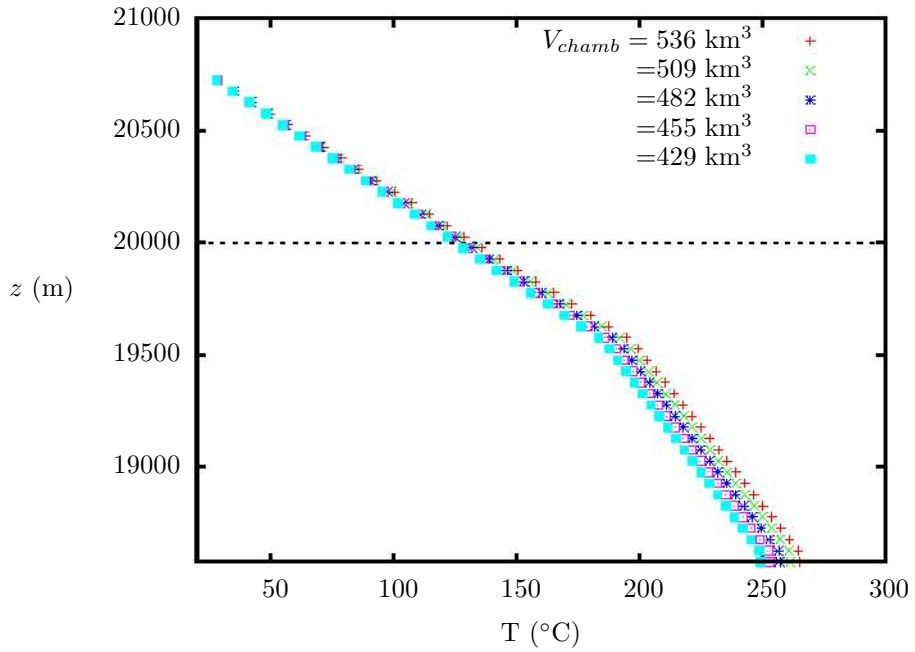

Figure 5.5: Geothermal gradients of well LV3 corresponding to five total chambers volume (models LTV-1.1 to LTV-1.5). Sea level is shown in dotted line.

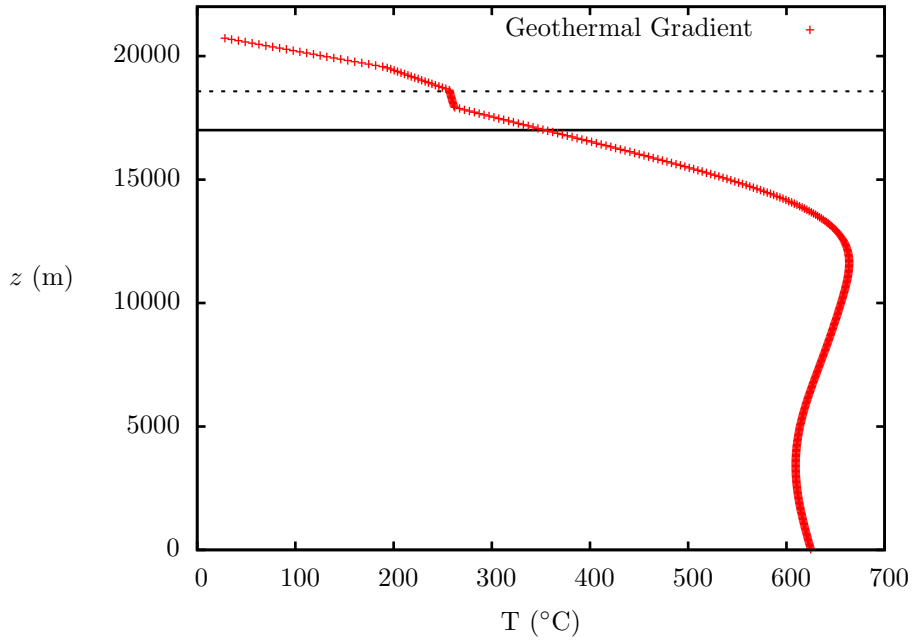

Figure 5.6: Geothermal gradient referred to the site of well LV3 obtained with the model LTV-1.3. The top of the chambers is shown in solid line. The depth of well LV3 is shown in dotted line. A high conductivity region is observed bellow the bottom of the well that simulates a convective zone.

5.3 Model calibration

Static formation temperatures (SFT) and homogenization temperatures of fluid inclusions published by Verma *et al.* [34] were used for model calibration. Five geothermal wells were analyzed (Table 5.2). Static formation temperatures and the lower homogenization temperature were used as reference to evaluate the results (Table 5.3). Small estimation errors are reported by Verma *et al.* [34] (up to 11 °C) based on quadratic regression models published by Andaverde *et al.* [35].

The agreement of the simulation results of a particular model (Table 5.1) with reference temperatures (SFT) was evaluated with ΔT_m that provides the mean difference between simulated and estimated formation temperatures ($\Delta T = T_{sim} - T_{estim}$) in the bottom of all the wells analyzed (five wells in this case; Equation 5.1).

$$\Delta T_m = \frac{\sqrt{\sum_{i=1}^{5} (T_{sim} - T_{estim})_i^2}}{5} \tag{5.1}$$

Table 5.2: SFT used for model calibration (from Verma *et al.* [34].)

Well	Elevation (m a.s.l)	Vertical Depth (m)	SFT (°C)	T_h range (°C)
LV1	741	1695	212	—
LV3	720	2150	—	261-263
LV4	720	2367	250	287-292
LV7	523	1250	—	207-213
LV8	725	985	162	—

The models with minimum ΔT_m in each depth series (3000, 3500 and 4000 m; Table 5.1) are presented in Table 5.3. According to these results, the best models lie between the cases LTV-1.5 and LTV-2.1. It is pertinent to mention that the model LTV-2.2 reported a slightly better result ($\Delta T_m = 5.17$) than the model LTV-1.1 ($\Delta T_m = 5.21$). As a first approximation, it was inferred that the chambers depth must be shallow, between 3000 and 3500 m b.s.l., and the total chamber volume must be up to 536 km^3.

Table 5.3: Comparison of estimated and simulated SFT (time step $\Delta T = 1.0 \times 10^{-3}$ and tolerance $\delta = 1.0 \times 10^{-6}$; $t^*_{cpu} \approxeq 1.0$ for all these models; all temperatures reported in °C).

	Reference	Simulated temperatures					
Well	Temperatures	LTV-1.5	ΔT	LTV-2.1	ΔT	LTV-3.1	ΔT
LV1	212	231	19	223	11	204	-8
LV3	261	262	1	252	-9	230	-31
LV4	250	263	13	254	4	231	-19
LV7	207	195	-12	188	-19	172	-35
LV8	162	164	2	159	3	146	-16
	ΔT_m=		5.21		4.85		10.7

Considering the results in Subsection 3.3.2 as a general behavior of this kind of problem (the same domain, mesh and initial and boundary conditions), it is assumed that a smaller Δt is important for a large simulation time in the LTV model. Because of this consideration, simulations of a set of six models (from LTV-1.1 to LTV-2.1; Table 5.1) were carried out using $\Delta T = 1.0 \times 10^{-4}$ m.y. and a tolerance $\delta = 1.0 \times 10^{-7}$.

Better model calibration and refined results were achieved (Tables 5.4 and 5.5). Models

LTV-1.3 and LTV-1.4 provided closer temperatures to the references than the model LTV-2.1 (Table 5.5), unlike the preliminary results. Considering that the model LTV-1.3 reported the best results, it is inferred a total chambers volume of about 482 km^3 with $d_{cham} = 3000$ m b.s.l..

Besides, in agreement with the preliminary results (Table 5.3), in this refined simulations the model LTV-2.1 produced smaller temperatures than the model LTV-1.5. Therefore, it is not expected an improvement in model calibration for $d_{cham} = 3500$ m b.s.l. with chambers volume smaller than 536 km^3.

Table 5.4: Calibration (ΔT_m) and computation time (t^*_{cpu}) of the models simulated with a time step $\Delta T = 1.0 \times 10^{-4}$ and tolerance $\delta = 1.0 \times 10^{-7}$.

Model	ΔT_m	t^*_{cpu}
LTV-1.1	5.82	7.8
LTV-1.2	4.98	8.0
LTV-1.3	4.48	7.8
LTV-1.4	4.52	8.7
LTV-1.5	4.81	6.4
LTV-2.1	5.47	6.5

Table 5.5: Simulated temperatures of selected models ($\Delta T = 1.0 \times 10^{-4}$ m.y.; $\delta = 1.0 \times 10^{-7}$).

	Reference	Simulated temperatures							
Well	Temperatures	LTV-1.3	ΔT	LTV-1.4	ΔT	LTV-1.5	ΔT	LTV-2.1	ΔT
LV1	212	227	15	223	11	219	7	218	6
LV3	261	257	-4	252	-9	249	-12	246	-15
LV4	250	258	8	254	4	250	0	247	-3
LV7	207	193	-14	190	-17	188	-19	186	-21
LV8	162	162	0	160	-2	157	-5	156	-6

Chapter 6

Conclusions

Here I present only the most important conclusions of this thesis. Specific conclusions are presented in respective chapters.

- A natural state simulation of the Las Tres Vírgenes geothermal field was achieved with good model calibration. The modeling of two magma chambers permitted a better reproduction of the volcanic history and distribution of mass of the heat source. Besides, the spherical modeling of the magma chambers led to more realistic heat flux patterns with respect to the cylindrical chamber used by TCHEMSYS.

- General guidelines for developing LTV numerical model were obtained from the study of TCHEMSYS model. Refining the mesh in z-axis provides better simulation results and permits a better comparison between simulated and estimated temperatures.

- It was observed a reduction of the simulated temperatures as the time step is reduced. This effect is increased with large simulation times. The evaluation of simulation results obtained with two different time steps was important for refining simulation results.

- The emplacement scheme used produced a directly proportional relation between BHT and the chamber volumes for a fixed depth.

- It is necessary to consider the topography of the geographic area for an accurate reproduction of the thermal regime in shallow depths. The temperature field is clearly affected by the topography in the geothermal area.
- The best model corresponded to a total chambers volume of about 482 km^3 and chambers depth of 3000 m b.s.l. with a maximum temperature in the LTV chamber of about 690 °C. Nevertheless, chambers depth of 3500 m with chambers volume of up to 536 km^3 also provided good agreement with static formation temperatures.

Appendix A

TCHEMSYS application. La Primavera caldera, Jalisco, Mexico.

The numbering of eleven pages of the in-press article are supplemented by the numbering of this thesis.

International Geology Review
2011, iFirst article, 1–11

Taylor & Francis
Taylor & Francis Group

Three-dimensional temperature field simulation of a cooling of a magma chamber, La Primavera caldera, Jalisco, Mexico

Surendra P. Verma[a]*, Usy C. Arredondo-Parra[a], Jorge Andaverde[b], Efraín Gómez-Arias[c] and Fernando J. Guerrero-Martínez[c]

[a]*Departamento de Sistemas Energéticos, Centro de Investigación en Energía, Universidad Nacional Autónoma de México, Temixco, Morelos 62580, Mexico;* [b]*Facultad de Ciencias Químicas, Universidad Veracruzana, Coatzacoalcos, Veracruz 96538, Mexico;* [c]*Posgrado en Ingeniería, Centro de Investigación en Energía, Universidad Nacional Autónoma de México, Temixco, Morelos 62580, Mexico*

(*Accepted 21 April 2011*)

The La Primavera caldera lies close to the triple junction of the Tepic-Zacoalco, Colima, and Chapala rifts in the western part of the Mexican Volcanic Belt. It is a promising geothermal field with 13 deep wells already drilled. We calculated solute geothermometric temperatures (Na–K, Na–Li, and SiO_2) from the chemistry of geothermal water samples; determined values are generally between 99°C and 202°C for springs and between 131°C and 298°C for wells. Thermal modelling is an important geophysical tool as documented in the study of this and other Mexican geothermal areas. Using the computer program TCHEMSYS, we report new simulation results of three-dimensional (3-D) thermal modelling of the magma chamber underlying this caldera through its entire eruptive history. Equations (quadratic fit) describing the simulated temperatures as a function of the age, volume and depth of the magma chamber are first presented; these indicate that both the depth and the age of the magma chamber are more important parameters than its volume. A comparison of 3-D modelling of the La Primavera and Los Humeros calderas also shows that the depth of the magma chamber is more important than its volume. The best model for the La Primavera caldera has 0.15 million years as the emplacement age of the magma chamber, its top at a depth of 4 km, and its volume as 600 km^3. Fresh magma recharge events within the middle part of the magma chamber were also considered at 0.095, 0.075, and 0.040 Ma. The simulation results were evaluated in the light of actually measured and solute geothermometric temperatures in five geothermal wells. Future work should involve a smaller mesh size of 0.050 or 0.10 km on each side (instead of 0.25 km currently used) and take into account the topography of the area and all petrogenetic processes of fractional crystallization, assimilation, and magma mixing as well as heat generation from natural radioactive elements.

Keywords: solute geothermometer; temperature field; modelling; geothermal field; magma chamber

Downloaded by [UNAM Ciudad Universitaria] at 09:58 13 December 2011

Introduction

Temperature field simulation from a magma chamber constitutes an important area of research to understand the origin and evolution of calderas and assess their geothermal potential (Spera *et al*. 1982; Giberti *et al*. 1984; Verma 1985a, 1985b; Tait 1988; Giberti and Sartoris 1989; Valentine 1992; Stimac *et al*. 2001). In Mexico, numerous studies (Verma 1985a; Verma *et al*. 1990; Castillo-Román *et al.* 1991; Verma and Andaverde 1996, 2007; Verma *et al*. 2011a) have been carried out, mainly in the Los Humeros caldera of the eastern part of the Mexican Volcanic Belt (MVB; see Figure 1).

The La Primavera caldera is situated in the western part of the MVB near the triple junction of three rifts or graben systems, namely, Tepic-Zacoalco rift, Colima rift, and Chapala rift (Figure 1). Exploratory well-drilling work to 2.986 km subsurface depth indicated high temperatures (Mahood 1977; Mahood *et al*. 1983; Villa Merlo *et al*. 1987; Yokoyama and Mena 1991; Maciel-Flores and Rosas-Elguera 1992).

The only available temperature field simulation study in this caldera (Verma and Rodríguez-González 1997) was carried out in two dimensions (2-D), assuming the top of the magma chamber at 5–7 km depth and horizontal dimensions of 10–12 km width. The resulting isotherms were qualitatively compared with the actually measured bottom hole temperatures.

In this work our aim was to carry out thermal simulation in three dimensions (3-D) of several different models of a magma chamber assumed to underlie this caldera as the primary heat source. The entire eruption history of the caldera was simulated for different models of the magma chamber (volume and depth), its emplacement age, as well as different physical properties of the region. These

*Corresponding author. Email: spv@cie.unam.mx

ISSN: 0020-6814 print/ISSN: 1938-2839 online
© 2011 Taylor & Francis
DOI: 10.1080/00206814.2011.585036
http://www.informaworld.com

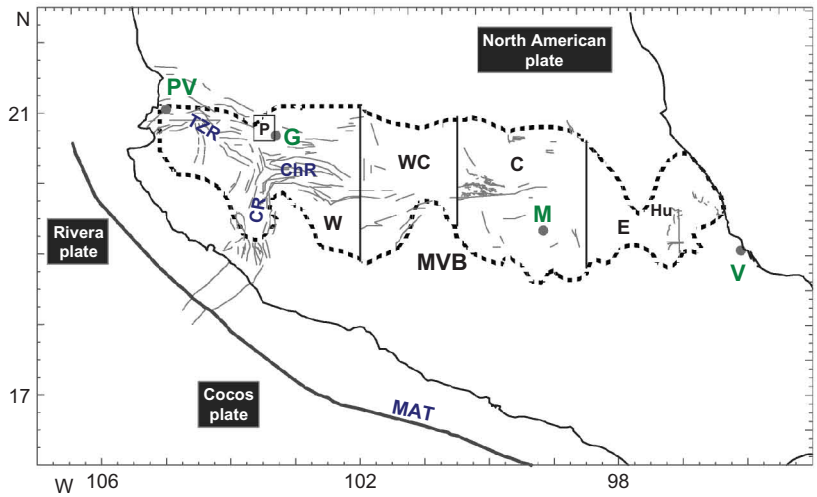

Figure 1. Location of the La Primavera caldera (P), Jalisco, in the western part of the Mexican Volcanic Belt (MVB; modified after Verma 2000). MAT, Middle America Trench; TZR, Tepic-Zacoalco rift; CR, Colima rift; ChR, Chapala rift; PV, Puerto Vallarta; V, Veracruz; G, Guadalajara; M, Mexico City; Hu, Los Humeros caldera; W, WC, C, and E refer to, respectively, the western, west-central, central, and eastern parts of the MVB. Major geological faults and fractures and the subdivision of the MVB (after Verma *et al*. 2011b) are also shown schematically.

Downloaded by [UNAM Ciudad Universitaria] at 09:58 13 December 2011

results enabled us to propose five equations that were used to understand the sensitivity of these parameters to the simulated temperature field.

Geological synthesis

The geology of the La Primavera caldera (about 12 km diameter) has been summarized by several researchers (Mahood 1977; 1980, 1981a, 1981b; Wright 1981; Mahood and Drake 1982; Mahood *et al*. 1983; Villa Merlo *et al*. 1987; Mahood and Halliday 1988; Michael 1988; Alatorre-Zamora and Campos-Enríquez 1991; Yokoyama and Mena 1991; Maciel-Flores and Rosas-Elguera 1992; Verma and Rodríguez-González 1997; Campos-Enríquez *et al*. 2005). Different eruptive events were dated by Mahood and Drake (1982) using the K–Ar method. These dates vary from about 0.145 to 0.025 Ma. Figure 2 presents a simplified geologic map of the area as well as the locations of drill wells.

The nature of regional basement in the La Primavera area is not clearly known because of an extensive, thick cover of younger volcanic rocks. Drilling (Figure 3) has revealed that the oldest units consist of granitic and granodioritic rocks mainly below about 3000 m subsurface depth. This deeper layer is overlain by dominantly andesitic rocks about 1150 m thick. The third lithologic unit about 100 m thick consists of rhyolites. The upper unit is a sequence of lithic tuffs and minor andesites of an average thickness of about 750 and 1000 m, respectively.

The La Primavera caldera is a very young (late Pleistocene) volcanic complex, in which the oldest pre-caldera lavas are about 65 m-thick peralkaline rhyolites at about 400 m depth. The earliest eruptions of pre-caldera lavas took place between about 0.145 and 0.100 Ma. The eruption of the caldera-forming event (40 km^3 of Tala tuff) occurred at about 0.095 Ma. Tala tuff and caldera-lake sediments overlie these peralkaline rocks. Soon afterwards, central domes and older ring domes (about 5 km^3) were emplaced. Eruption of younger ring domes (about 3 km^3) took place at about 0.075 Ma, which was followed by uplift and final eruption of southern arc lavas (about 7 km^3) at about 0.060–0.025 Ma (Figure 3).

Geothermometric temperatures

Thermal manifestations (hot springs with actually measured temperatures around 65°C associated with geological faults and fumaroles related to caldera collapse and to later magma insurgence) were also studied by Mahood *et al*. (1983) for estimating subsurface temperatures from solute geothermometers. Using solute geothermometers for spring water, Mahood *et al*. (1983; their table 3) reported moderately high subsurface temperatures at La Primavera (148–199°C from a Na–K geothermometer (White 1970; Fournier 1979) and 93–163°C from a Na–K–Ca geothermometer (Fournier and Truesdell 1973; Fournier and Potter 1979)). The $\delta^{18}O$ (SO_4–H_2O) geothermometer (McKenzie and Truesdell 1977) provided slightly higher temperature estimates of 184–192°C.

Our own estimates of geothermometric temperatures of spring data presented by Mahood *et al*. (1983) through the computer program SolGeo (Verma *et al*. 2008) provided

Downloaded by [UNAM Ciudad Universitaria] at 09:58 13 December 2011

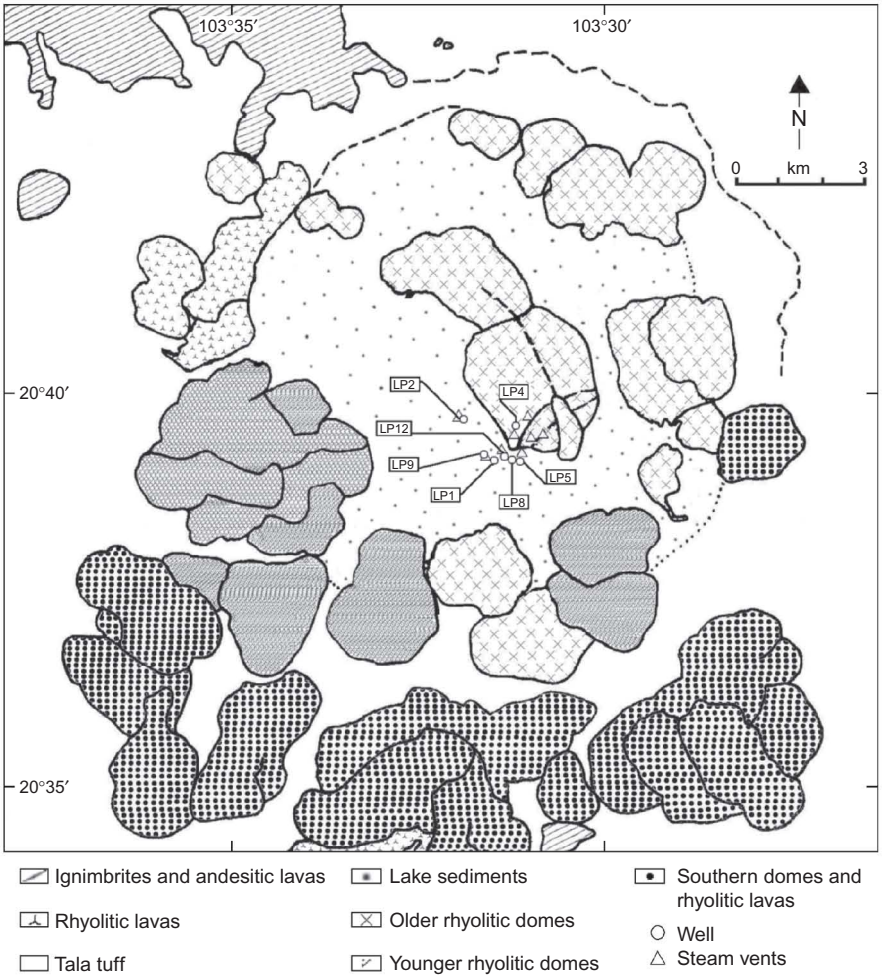

Figure 2. Simplified surface geology of the La Primavera caldera, modified after Mahood (1977, 1980, 1981a, 1981b). The wells referred to in the text are identified.

the following results (Table 1, only those temperatures for which respective errors could be determined are tabulated): (1) for Na–K geothermometers from 140°C ± 43°C to 199°C ± 53°C (Fournier 1979), from 146°C ± 35°C to 202°C ± 42°C (Verma and Santoyo 1997), 102°C ± 8°C to 170°C ± 11°C (Díaz-González *et al*. 2008), and 99°C ± 7°C to 167°C ± 9°C (these temperatures were calculated from the equation reported by Verma and Díaz-González 2011); (2) for Na–Li geothermometers from 84°C ± 22°C to 166°C ± 30°C (Fouillac and Michard 1981) and from 93°C ± 20°C to 176°C ± 27°C (Verma and Santoyo 1997); and (3) for SiO_2 geothermometers from 149°C ± 4°C to 190°C ± 5°C (Fournier and Potter 1982) and from 149°C ± 2°C to 189°C ± 3°C (Verma and Santoyo 1997). Although the various estimates of Na–K and Na–Li geothermometers are in general consistent, SiO_2 geothermometric temperatures are somewhat higher, especially when the minimum values are compared.

We also used SolGeo for calculating geothermometric temperatures for wells LP2, LP9, LP1, LP8, LP5, and LP4 (Figure 2) and obtained the following results (Table 1, well data from Mahood *et al*. 1983; Villa Merlo *et al*. 1987): (1) Na–K geothermometers from 168°C ± 48°C to 296°C ± 71°C (Fournier 1979), 173°C ± 38°C to 295°C ± 56°C (Verma and Santoyo 1997), 134°C ± 9°C to 298°C ± 16°C (Díaz-González *et al*. 2008), and 131°C ± 8°C to 295°C ± 14°C (Verma and Díaz-González 2011); (2) Na–Li geothermometers for only two wells (LP2 and LP1) from 85°C ± 22°C to 323°C ± 48°C (Fouillac and Michard 1981) and from 95°C ± 20°C to 331°C ± 43°C (Verma and Santoyo 1997); and (3) SiO_2 geothermometers from 190°C ± 5°C to 289°C ± 16°C (Fournier and Potter 1982) and from 189°C ± 3°C to 289°C ± 4°C (Verma and Santoyo 1997).

The actually measured bottom hole temperatures for LP2, LP9, LP1, LP8, and LP5 were between 210°C and

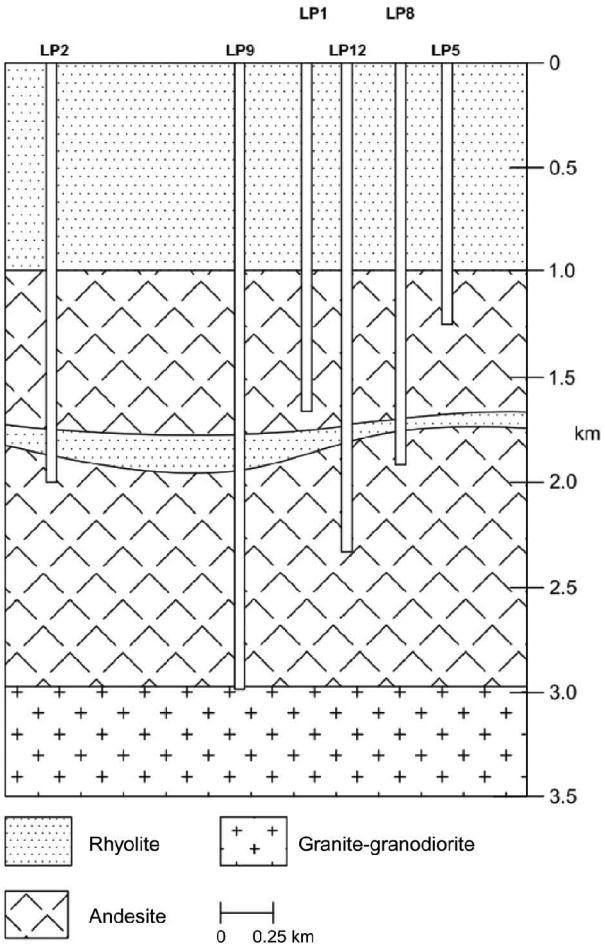

Figure 3. Simplified lithology from the drilling information of wells in the La Primavera caldera (modified after Yokoyama and Mena 1991). The wells (LP – La Primavera) along the approximate section are numbered as follows: LP2 (about 2.005 km depth), LP9 (about 2.986 km depth), LP1 (about 1.822 km depth), LP12 (about 2.560 km depth), LP8 (about 1.861 km depth), LP5 (about 1.215 km depth), and LP4 (about 0.668 km depth; this well is not shown because it lies far away from the section of this figure). The lowermost stratum is assumed to be of granitic and granodioritic composition.

303°C (Villa Merlo *et al*. 1987). For comparison, the solute geothermometric temperatures varied from 131°C to 298°C for Na–K, from 85°C to 331°C for Na–Li, and from 189°C to 289°C for SiO_2.

Conceptual model

Figure 4 presents a simplified conceptual model for simulating temperature field distribution in the La Primavera caldera. The diameter of the magma chamber was assumed to be 12 km, similar to the caldera diameter. It was supposed to be surrounded by granitic and granodioritic rocks actually encountered at deeper levels during drilling operations. For simulation purposes, the drill well geology (Figure 3) was simplified as three distinct layers, the deepest one consisting of granitic–granodioritic rocks. The geothermal reservoir was assumed to be at 2–3 km subsurface depth. The shallowest layer was assumed to be dominantly rhyolite.

Thermal modelling

We used the computer program TCHEMSYS (*T*hermal and *CHE*mical *M*odeling of a Volcanic-Geothermal *SYS*tem) by Verma and Andaverde (2007), written in Fortran and consisting of 8 modules that can simulate thermal and chemical evolution of a cylindrical magma chamber in a maximum domain of 30 km in horizontal directions and 20 km in the vertical direction, that is, in a space of 30 × 30 × 20 (18,000) km^3. The 3-D heat flow and chemical mass-balance equations are solved by the control volume method, with the volume size of 0.250 km in each direction, that is, 0.250 × 0.250 × 0.250 (0.015625) km^3 amounting to 1,152,000 control volumes for the entire simulated region.

Verma and Andaverde (2007) used this program to simulate the temperature field and chemical compositions in the Los Humeros geothermal field from the cooling of a magma chamber. The results were validated by comparing the simulated temperatures with the stabilized temperatures from actual bottom hole temperature measurements reported by Andaverde *et al*. (2005) and the simulated major-element chemistry with that of the most-voluminous caldera-forming ignimbrite reported by Verma (2000). More recently, Verma *et al*. (2011a) also used TCHEMSYS to understand the dependence of spatial distribution of simulated temperatures on magma chamber volume and depth.

In this work, the HEAT_FORMING module of TCHEMSYS (for details on this program, see Verma *et al.* 2011a) was used to simulate the temperature field in 3-D for a magma chamber underlying the La Primavera caldera. The initial and boundary conditions as well as other information on the simulation models of the La Primavera caldera are summarized in Table 2. The input data for the program come from three files, which contain information on boundary conditions, emplacement conditions, and mesh construction (Table 2).

To simulate and compare the results of different magma chamber models, the volume of the magma chamber was varied from 500 to 700 km^3, with its top at depths varying from 4 to 7 km. Correspondingly, the depth of the centroid of the magma chamber ranged from 6.125 to 9.875 km. These chamber volume estimates are reasonable from the geochemical modelling reported by Verma (1985b) and the erupted volumes of differentiated magmas which amount to about 45 km^3 for the main caldera-forming event and the related domes emplaced during practically the same

Downloaded by [UNAM Ciudad Universitaria] at 09:58 13 December 2011

Table 1. Geothermometric temperatures (°C) of springs and wells from the La Primavera geothermal field.

	Na–K				Na–Li		SiO_2	
Spring/well	F79	VS97	DSR08	VD11	FM81	VS97	FP82	VS97
Springs								
Orfanato	151 (±45)	157 (±36)	114 (±9)	111 (±8)	154 (±29)	164 (±26)	187 (±5)	186 (±3)
Río Caliente	148 (±45)	154 (±36)	111 (±9)	108 (±7)	154 (±28)	163 (±26)	190 (±5)	189 (±3)
Agua Brava	159 (±46)	164 (±37)	124 (±9)	121 (±8)	155 (±29)	165 (±26)	183 (±5)	183 (±3)
Arroyo Verde	151 (±45)	156 (±36)	114 (±9)	111 (±8)	153 (±28)	162 (±26)	186 (±5)	185 (±3)
Agua Caliente	140 (±43)	146 (±35)	102 (±8)	99 (±7)	166 (±30)	176 (±27)	172 (±5)	172 (±3)
Cañón de las flores	199 (±53)	202 (±42)	170 (±11)	167 (±9)	84 (±22)	93 (±20)	149 (±4)	149 (±2)
Wells								
LP2	168 (±48)–175 (±49)	173 (±38)–179 (±39)	134 (±9)–142 (±10)	131 (±8)–139 (±8)	85 (±22)–175 (±31)	95 (±20)–185 (±28)	215 (±7)–289 (±16)	215 (±3)–289 (±4)
LP9	296 (±71)	295 (±56)	298 (±16)	295 (±14)	–	–	–	–
LP1	262 (±64)–278 (±67)	262 (±51)–278 (±53)	251 (±14)–273 (±15)	248 (±12)–270 (±13)	323 (±48)	331 (±43)	280 (±15)	281 (±4)
LP8	281 (±68)	280 (±54)	276 (±15)	273 (±13)	–	–	–	–
LP5	197 (±52)–259 (±63)	201 (±42)–260 (±50)	169 (±11)–247 (±14)	166 (±9)–244 (±12)	–	–	236 (±8)–283 (±15)	236 (±3)–283 (±4)
LP4	199 (±53)	203 (±42)	171 (±11)	168 (±9)	–	–	190 (±5)	189 (±3)

Notes: F79, Fournier (1979); VS97, Verma and Santoyo (1997); DSR08, Díaz-González *et al*. (2008); VD11, Verma and Díaz-González (2011); FM81, Fouillac and Michard (1981); FP82, Fournier and Potter (1982).

Downloaded by [UNAM Ciudad Universitaria] at 09:58 13 December 2011

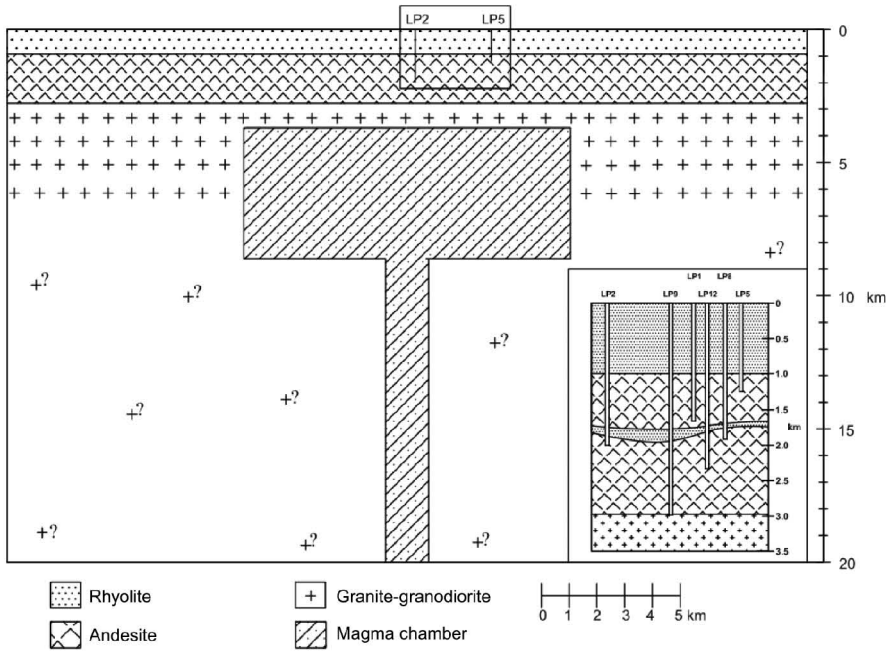

Figure 4. Simplified geological model of geothermal reservoir and magma chamber in the La Primavera caldera. The question marks in the lowermost stratum (assumed to be an intrusive body) represent its hitherto unknown chemical and mineralogical characteristics.

Downloaded by [UNAM Ciudad Universitaria] at 09:58 13 December 2011

Table 2. Initial and boundary conditions for the model of the La Primavera caldera, Jalisco, Mexico.

Physical property (units)	Emplacement of magma chamber
Boundary conditions	
Surface temperature (T_s) (°C)	25
Temperature gradient (ΔT_g) (°C/km)	30
Emplacement conditions	
Volume (V_{cham}) (km^3)	500–700
Radius (r_{cham}) (km)	6
Depth of the top the chamber (d_{cham}) (km)	4–7
Magma emplacement temperature (T_{cham}) (°C)	1350
Mesh construction	
Length – x (km)	30
Number of control volumes in x-direction	120
Length – y (km)	30
Number of control volumes in y-direction	120
Number of geological strata	5
Control volume (δx, δy, δz) (km)	(0.25, 0.25, 0.25)
Geological strata (1–5)	
Stratum 1 (deepest layer) width (km)	17.00
Rock thermal conductivity (W/mK)	2.60
Specific heat (J/kg K)	1073
Density (kg/m^3)	2460
Stratum 2 width (km)	1.15
Rock thermal conductivity (W/mK)	1.28
Specific heat (J/kg K)	1151
Density (kg/m^3)	2180
Stratum 3 width (km)	0.10
Rock thermal conductivity (W/mK)	2.68
Specific heat (J/kg K)	1074
Density (kg/m^3)	2460
Stratum 4 width (km)	0.75
Rock thermal conductivity (W/mK)	1.28
Specific heat (J/kg K)	1073
Density (kg/m^3)	2460
Stratum 5 (shallowest layer) width (km)	1.00
Rock thermal conductivity (W/mK)	2.08
Specific heat (J/kg K)	900
Density (kg/m^3)	2200
Time constraints	
Time step (Δt) (year)	250
Total simulation time (t) (Ma)	0.095–0.24

time at about 0.095 Ma. The radius of the cylindrical magma chamber (6 km) was assumed to be similar to that of the caldera. Although only highly differentiated rhyolitic magmas are emplaced within the caldera (Mahood 1977; Mahood and Hildreth 1983; Mahood *et al.* 1983; Mahood and Halliday 1988), the latter is surrounded by volcanic centres that have erupted basic magmas (Mahood *et al.* 1983; Mahood and Halliday 1988; Michael 1988). Therefore, it is reasonable to assume that the magma chamber was initially formed by mantle-derived basic magmas whose initial temperature was also assumed at about 1350°C (Nielsen 1988). This assumption is similar to that used for the magma chamber in the Los Humeros caldera (Ferriz 1985; Verma *et al.* 2011a).

Table 3. Emplacement conditions for sensitivity evaluation of the La Primavera caldera, Jalisco, Mexico.

Physical property (units)	Emplacement of magma chamber
Depth of the top the chamber ($d_{t_{cham}}$) (km)	4–7
Depth of the chamber centroid ($d_{c_{cham}}$) (km)	6.125–9.875
Volume (V_{cham}) (km^3)	500–700
Thickness (E_{cham}) (km)	4.4–6.2
Radius (r_{cham}) (km)	6
Magma emplacement temperature (T_{cham}) (°C)	1350
Time of emplacement (Ma)	0.095–0.240
Time step (year)	250

For simulating the temperature field from different models (Table 3), the time of emplacement of the magma chamber in the La Primavera was assumed to be 0.240, 0.120, and 0.095 Ma. The depth of the top of the magma chamber was assigned values of 4, 5, 6, and 7 km. The volume of the magma chamber was modelled as three different values of 500, 600, and 700 km^3. For changing magma chamber volume for a given depth of the top of the chamber, its diameter was assumed to be fixed, that is, the chamber was assumed to grow at deeper levels. Therefore, we also report the subsurface depths of chamber centroid (Table 3).

Thus, TCHEMSYS was run 36 times to simulate the temperature field for all combinations of emplacement time, magma chamber depth (either as the depth of the top of the magma chamber or as that of its centroid), and its volume. From these simulated temperatures, best-fit equations were obtained for predicting the temperatures as a function of the emplacement time, chamber depth, and volume variables.

Additional simulations were then carried out using the selected parameters of magma chamber and effective thermal conductivity values of the three layers (Figure 4), which varied as multiples of actual rock thermal conductivity data. These higher conductivity values were necessary to take into account the contribution of geological faults and fractures as well as varying porosity of the rocks. The actual distribution of these properties is difficult to establish, and therefore, different combinations of the effective thermal conductivity values were used for simulation. Besides fractional crystallization and assimilation of country rocks, an additional petrogenetic process of magma recharge was also considered.

Results and discussion

Best-fit equations

The results of temperature simulation at the base of the La Primavera geothermal reservoir (assumed from 2 to

Downloaded by [UNAM Ciudad Universitaria] at 09:58 13 December 2011

Table 4. Temperature at the base of the geothermal reservoirs (3 km depth) resulting from conductive cooling of a magma chamber in the La Primavera caldera, Jalisco, Mexico.

Emplacement time t (Ma)	Depth of chamber top $d_{t_{cham}}$ (km)	Chamber centroid $d_{c_{cham}}$ (km)	Volume V_{cham} (km^3)	Temperature (°C)
0.095	4	6.125	500	338
0.095	5	7.125	500	179
0.095	6	8.125	500	128
0.095	7	9.125	500	120
0.095	4	6.625	600	333
0.095	5	7.625	600	175
0.095	6	8.625	600	127
0.095	7	9.625	600	119
0.095	4	6.875	700	278
0.095	5	7.875	700	154
0.095	6	8.875	700	123
0.095	7	9.875	700	119
0.120	4	6.125	500	360
0.120	5	7.125	500	204
0.120	6	8.125	500	138
0.120	7	9.125	500	122
0.120	4	6.625	600	357
0.120	5	7.625	600	200
0.120	6	8.625	600	137
0.120	7	9.625	600	121
0.120	4	6.875	700	306
0.120	5	7.875	700	175
0.120	6	8.875	700	130
0.120	7	9.875	700	120
0.240	4	6.125	500	400
0.240	5	7.125	500	273
0.240	6	8.125	500	189
0.240	7	9.125	500	145
0.240	4	6.625	600	402
0.240	5	7.625	600	272
0.240	6	8.625	600	188
0.240	7	9.625	600	144
0.240	4	6.875	700	366
0.240	5	7.875	700	246
0.240	6	8.875	700	173
0.240	7	9.875	700	138

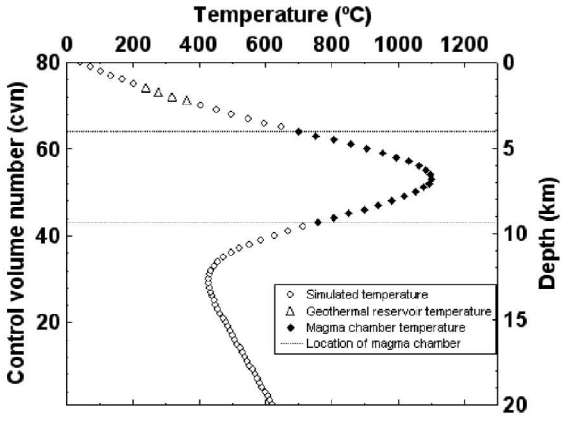

Figure 5. Temperature field distribution as a function of depth in kilometres (vertical axis at the right side of the diagram) or as the control volume number (cvn; vertical axis at the left side of the diagram). The magma chamber is schematically shown by dotted lines. The diagram shows the temperature distribution along a vertical line (coordinates 80, 1 in the control volume space) of 20 km depth, at the centre of the chamber ($x = 60$ and $y = 60$), that is, between the surface (coordinates 60, 60, 80) and the deepest part of the simulated volume (60, 60, 1). Note that the thermal anomaly due to the emplacement and cooling of the magma chamber is still observed within the magma chamber (see filled diamonds) as well as both above and below it (see open circles). Open triangles show the temperature field in the geothermal reservoir.

3 km subsurface depths) for these different magma chamber models are summarized in Table 4. Qualitatively, for any given magma chamber depth and volume, an increase in emplacement time (t) from 0.095 to 0.240 Ma causes an increase in the temperature at 3 km subsurface depth. For example, for magma chamber of 500 km^3 volume (V_{cham}) emplaced at 4 km depth (top of the magma chamber, $d_{t_{cham}}$) or equivalently at 6.125 km depth of chamber centroid ($d_{c_{cham}}$), the temperature increases from about 338°C for emplacement time of 0.095 Ma to 360°C for 0.120 Ma and to 400°C for 0.240 Ma (Table 4).

Figure 5 shows the results for one of the models, in which initial time of 0.120 Ma, volume of 600 km^3, and chamber depth of 4 km were assumed. Thus, it appears that the magma chamber is still maintained at high temperatures (about 700–1100°C), the centre of the magma chamber being at about 1100°C.

For a given t and V_{cham}, an increase in $d_{t_{cham}}$ from 4 to 7 km significantly decreases the simulated temperature at 3 km depth (Table 4). For example, for t of 0.095 Ma and V_{cham} of 500 km^3, the simulated temperature decreases from 338°C for $d_{t_{cham}}$ of 4 km, to 179°C for $d_{t_{cham}}$ of 5 km, to 128°C for $d_{t_{cham}}$ of 6 km, and to 120°C for $d_{t_{cham}}$ of 7 km (Table 4).

Finally, for a given t and $d_{t_{cham}}$ or $d_{c_{cham}}$, an increase in magma chamber volume slightly decreases the temperature at 3 km subsurface depth. For example, for t of 0.095 Ma and $d_{t_{cham}}$ of 4 km or $d_{c_{cham}}$ of 6.125 km, the simulated temperature at 3 km depth decreases from 338°C for V_{cham} of 500 km^3 to 333°C for V_{cham} of 600 km^3 and to 278°C for V_{cham} of 700 km^3. This may be partly due to our magma chamber model, in which it is assumed that the increase in chamber volume at a given depth of the chamber top increases the depth of the chamber centroid, that is, the chamber is supposed to maintain its diameter and grows in the vertical direction only towards the deeper levels.

The best-fit equations for predicting temperatures at the base of the geothermal reservoir in terms of these parameters were obtained to quantitatively interpret the simulated data (Table 4). Two regression equations (1) and (2) for these subsurface temperatures, denominated

$T_{1(Z=3\ \mathrm{km})}$ for Equation (1) and $T_{2(Z=3\ \mathrm{km})}$ for Equation (2), respectively, were obtained as follows:

$$T_{1(\mathrm{Z=3km})} = (1110 \pm 230) + (900 \pm 700)t - (1400 \pm 2100)t^2 + (1.04 \pm 0.70)V_{\mathrm{cham}} - (1.0 \times 10^{-3} \pm 0.6 \times 10^{-3})V_{\mathrm{cham}}^2 - (400 \pm 30)d_{\mathrm{t_{cham}}} + (29.92 \pm 2.73)d_{\mathrm{t_{cham}}}{}^2 \quad (1)$$

$$T_{2\ (Z=3\mathrm{km})} = (1280 \pm 300) + (900 \pm 900)t - (1400 \pm 2500)t^2 + (2.77 \pm 0.85)V_{\mathrm{cham}} - (2.2 \times 10^{-3} \pm 0.7 \times 10^{-3})V_{\mathrm{cham}}^2 - (443 \pm 44)d_{\mathrm{c_{cham}}} + (23.04 \pm 2.74)d_{\mathrm{c_{cham}}}^2 \quad (2)$$

The quality of these best-fit equations is characterized by multiple correlation coefficient (R^2; Bevington and Robinson 2003) values of 0.97444 and 0.96191, respectively, for Equations (1) and (2). The regression analysis and examination of errors of the coefficients reveal that both intercept and $d_{\mathrm{t_{cham}}}$ are statistically significant at 99% confidence level in Equation (1) whereas intercept, V_{cham}, and $d_{\mathrm{c_{cham}}}$ are so in Equation (2). Further, the sizes of the coefficients indicate that the temperature at the base of the geothermal reservoir shows greater dependence on both t and $d_{\mathrm{t_{cham}}}$ (or $d_{\mathrm{c_{cham}}}$) than on V_{cham}. These results are consistent with similar thermal modelling of the magma chamber in Los Humeros geothermal field (Verma *et al*. 2011a), in which the greater importance of the magma chamber depth was suggested as compared with its volume.

Therefore, to better compare our simulation results for the La Primavera caldera with the Los Humeros caldera, we developed the following three regression equations for each emplacement time (Table 4; Equations (3–5), with R^2 values of 0.97380, 0.98544, 0.99714, respectively).

$$T_{(t=0.095\mathrm{Ma})} = (1300 \pm 400) + (0.95 \pm 1.26)V_{\mathrm{cham}} - (8.87 \times 10^{-4} \pm 10.5 \times 10^{-4})V_{\mathrm{cham}}^2 - (450 \pm 50)d_{\mathrm{t_{cham}}} + (35.1 \pm 5.0)d_{\mathrm{t_{cham}}}^2 \quad (3)$$

$$T_{(t=0.12\mathrm{Ma})} = (1300 \pm 325) + (1.02 \pm 1.02)V_{\mathrm{cham}} - (9.4 \times 10^{-4} \pm 8.5 \times 10^{-4})V_{\mathrm{cham}}^2 - (441 \pm 44)d_{\mathrm{t_{cham}}} + (33.55 \pm 4.02)d_{\mathrm{t_{cham}}}^2 \quad (4)$$

$$T_{(t=0.24\mathrm{Ma})} = (1004 \pm 155) + (1.15 \pm 0.49)V_{\mathrm{cham}} - (1.04 \times 10^{-3} \pm 0.41 \times 10^{-3})V_{\mathrm{cham}}^2 - (314.5 \pm 21.2)d_{\mathrm{t_{cham}}} + (21.1 \pm 1.9)d_{\mathrm{t_{cham}}}^2 \quad (5)$$

These equations also show that the depth of the magma chamber is a more important parameter than its volume.

For comparison, the simulation results for the Los Humeros caldera (Verma *et al*. 2011a) were used to obtain the following regression equation ($R^2 = 0.84332$) for the temperature at the base of the geothermal reservoir ($z = 3$ km) in the Los Humeros caldera ($T_{(\mathrm{LHC})}$):

$$T_{(\mathrm{LHC})} = (375 \pm 108) - (3.4 \times 10^{-3} \pm 0.2)V_{\mathrm{cham}} + (1.1 \times 10^{-7} \pm 7.4 \times 10^{-5})V_{\mathrm{cham}}^2 - (61.8 \pm 7.4)d_{\mathrm{t_{cham}}} + (3.69 \pm 0.49)d_{\mathrm{t_{cham}}}^2 \quad (6)$$

These results for the La Primavera and Los Humeros geothermal fields are in general consistent with the interpretation that the depth of the magma chamber is more important than its volume.

The best simulated model

These 36 simulated models used for obtaining the best-fit equations were also evaluated by comparing the simulated temperatures with the actually measured borehole temperatures (Villa Merlo *et al*. 1987). The best models are summarized in Figure 6 and Table 5. Three of these models (A–C) were, in fact, selected from these 36 simulations, with the additional process of magma recharge at 0.095 Ma and modification of physical properties to take into account more efficient heat transfer processes in the geothermal reservoir (see Figure 6 for more details on these models). Because even these models did not fully reproduce the measured temperatures (Table 5), we present a final model (D) (emplacement time 0.150 Ma, chamber volume 600 km^3, chamber depth 4 km, magma recharge at 0.095, 0.075, and 0.040 Ma, higher conductivity in both the geothermal reservoir and other geological structures; see Figure 6) which provided somewhat better agreement of the simulated temperatures with the measured and geothermometric temperatures.

Finer mesh construction (e.g. 0.050 or 0.100 km on each side instead of 0.250 km currently used) could provide more consistent results with the measured subsurface temperatures. The actual topography of the simulated region will have to be taken into consideration instead of the presently assumed sub-horizontal surface. Additionally, all petrogenetic processes such as fractional crystallization, assimilation, and magma mixing as well as heat generation

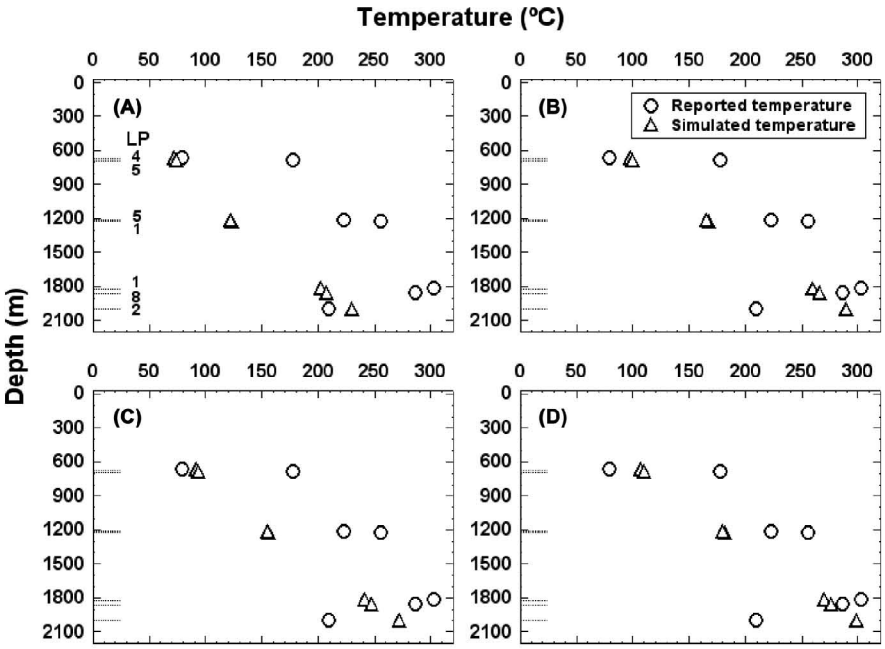

Figure 6. Comparison of simulated temperatures with the measured temperatures in La Primavera geothermal wells LP1, LP2, LP4, LP5, and LP8 (note the approximate depths in (A), where measured temperatures were reported, and see Figures 2 and 3 for locations of wells). The symbols used are shown as inset in (B). For rock thermal conductivity data see Table 2 and for effective conductivity as multiples of rock conductivities see Verma *et al*. (1990) or Castillo-Román *et al*. (1991) and references therein. The geothermal reservoir models were as follows: (A) magma chamber emplacement time (t), its top ($d_{t_{cham}}$), and its volume (V_{cham}) were, respectively, 0.120 Ma, 4 km depth, and 500 km^3; magma recharge volume (mag_r) of 5% magma chamber volume at 0.095 Ma; assumed reservoir (2–3 km depth; ek_{res}) effective conductivity of 10 times the rock conductivity; and of the other two layers (upper 0–2 km of effective conductivity ek_{ul} and lower >3 km depth of effective conductivity ek_{ll}) of 1.5 times the respective rock conductivity. (B) Values of t, $d_{t_{cham}}$, and V_{cham} were, respectively, 0.120 Ma, 4 km depth, and 500 km^3; mag_r of 10% magma chamber at 0.095 Ma; assumed ek_{res} of 20 times the rock conductivity; and both ek_{ul} and ek_{ll} of 4 times the respective rock conductivity. (C) Values of t, $d_{t_{cham}}$, and V_{cham} were, respectively, 0.120 Ma, 4 km depth, and 500 km^3; mag_r of 5% magma chamber at 0.095 Ma; assumed ek_{res} of 20 times the rock conductivity; and both ek_{ul} and ek_{ll} of 4 times the respective rock conductivity. (D) Values of t, $d_{t_{cham}}$, and V_{cham} were, respectively, 0.15 Ma, 4 km depth, and 600 km^3; mag_r of 10% magma chamber at 0.095 Ma; mag_r of 5% magma chamber at 0.075 and 0.040 Ma; assumed ek_{res} of 20 times the rock conductivity; and both ek_{ul} and ek_{ll} of 4 times the respective rock conductivity values.

Downloaded by [UNAM Ciudad Universitaria] at 09:58 13 December 2011

from radioactive elements naturally present in rocks should be taken into account. Besides, convection processes in the geothermal reservoir will have to be simulated. We also envisage the need of running TCHEMSYS in an automatic way, which could efficiently provide the best model(s) for each application. Unfortunately, in order to achieve these goals, we would need better computing facilities than those currently available to us. On the other hand, stabilized

Table 5. Measured and geothermometric (Na–K and SiO_2) temperatures versus temperature resulting from conductive cooling of a magma chamber in the La Primavera caldera (LPC), Jalisco, Mexico.

Well	Depth (km)	Measured temperature (°C)	Geothermometric temperature (°C)	Simulated temperature Model A (°C)	Simulated temperature Model B (°C)	Simulated temperature Model C (°C)	Simulated temperature Model D (°C)
LP2	2000	210	131 – 289	230	290	272	299
LP1	1226	256	–	124	168	156	182
LP1	1822	303	248 – 281	203	260	242	270
LP8	1861	287	273 – 281	209	266	248	276
LP5	690	178		74	100	94	110
LP5	1215	223	166 – 283	123	166	155	180
LP4	668	80	168 – 203	72	98	92	107

formation temperatures (Andaverde *et al*. 2005) will be necessary for a better comparison of the results.

Conclusions

Using 3-D simulations of the La Primavera caldera, we present two equations describing the simulated temperature at the base of the geothermal reservoir as a function of the age, volume, and depth of the magma chamber, as well as three equations for its volume and depth. The best model was obtained for a magma chamber emplacement age of 0.15 million year, with its top at a depth of 4 km, and a volume of 600 km^3. Our temperature simulation results were evaluated in the light of the actually measured temperatures in five geothermal wells (Table 5, model D).

Acknowledgements

Efraín Gómez-Arias and Fernando Guerrero-Martínez benefited from doctoral and master's fellowships from Conacyt, respectively, and Usy C. Arredondo-Parra did so partly from Sistema Nacional de Investigadores as Ayudantes de Investigador Nacional nivel 3. Jorge Andaverde is grateful to his university for granting him permission to periodically travel to Morelos and participate in this research. We also thank Carlos García Sánchez and Luis Eduardo Aguilar Pavón for help with the preparation of Figures 3 and 4. We are grateful to Oscar Fernando Silva Aguilar for kindly reviewing an earlier version of this article.

References

Alatorre-Zamora, M.A., and Campos-Enríquez, J.O., 1991, La Primavera caldera (Mexico): Structure inferred from gravity and hydrogeological considerations: Geophysics, v. 56, p. 992–1002.

Andaverde, J., Verma, S.P., and Santoyo, E., 2005, Uncertainty estimates of static formation temperatures in boreholes and evaluation of regression models: Geophysical Journal International, v. 160, p. 1112–1122.

Bevington, P.R., and Robinson, D.K., 2003, Data reduction and error analysis for the physical sciences: Boston, MA, McGraw-Hill, 320 p.

Campos-Enríquez, J.O., Domínguez-Méndez, F., Lozada-Zumaeta, M., Morales-Rodríguez, H.F., and Andaverde-Arredondo, J.A., 2005, Application of the Gauss theorem to the study of silicic calderas: The calderas of La Primavera, Los Azufres, and Los Humeros (Mexico): Journal of Volcanology and Geothermal Research, v. 147, p. 39–67.

Castillo-Román, J., Verma, S.P., and Andaverde, J., 1991, Modelación de temperaturas bajo la caldera de Los Humeros, Puebla, México, en términos de profundidad de la cámara magmática: Geofísica Internacional, v. 30, p. 149–172.

Díaz-González, L., Santoyo, E., and Reyes-Reyes, J., 2008, Tres nuevos geotermómetros mejorados de Na/K usando herramientas computacionales y geoquimiométricas: Aplicación a la predicción de temperaturas de sistemas geotérmicos: Revista Mexicana de Ciencias Geológicas, v. 25, p. 465–482.

Ferriz, H., 1985, Zoneamiento composicional y mineralógico en los productos eruptivos del centro volcánico de Los Humeros, Puebla, México: Geofísica Internacional, v. 24, p. 97–157.

Fouillac, C., and Michard, G., 1981, Sodium/lithium ratio in water applied to geothermometry of geothermal reservoirs: Geothermics, v. 10, p. 55–70.

Fournier, R.O., 1979, A revised equation for the Na/K geothermometer: Geothermal Resources Council Transactions, v. 3, p. 221–224.

Fournier, R.O., and Truesdell, A.H., 1973, An empirical Na-K-Ca geothermometer for natural waters: Geochimica et Cosmochimica Acta, v. 37, p. 1255–1275.

Fournier, R.O., and Potter, R.W., II, 1979, Magnesium correction to the Na-K-Ca chemical geothermometer: Geochimica et Cosmochimica Acta, v. 43, p. 1543–1550.

Fournier, R.O., and Potter, R.W., II, 1982, A revised and expanded silica (quartz) geothermometer: Geothermal Resources Council Bulletin, v. 11, p. 3–12.

Giberti, G., Moreno, S., and Sartoris, G., 1984, Thermal history of Phlegraean fields (Italy) in the last 50,000 years: A schematic numerical model: Bulletin Volcanologique, v. 47, p. 331–341.

Giberti, G., and Sartoris, G., 1989, Evaluation of approximations in modeling the thermal history of a volcanic area: Journal of Volcanology and Geothermal Research, v. 36, p. 233–240.

Maciel-Flores, R., and Rosas-Elguera, J., 1992, Modelo geológico y evaluación del campo geotérmico La Primavera, Jal. México: Geofísica Internacional, v. 31, p. 359–370.

Mahood, G.A., 1977, A preliminary report on the comenditic dome and ash flow complex of Sierra La Primavera, Jalisco, Mexico: Revista del Instituto de Geología UNAM, v. 1, p. 177–190.

Mahood, G.A., 1980, Geological evolution of a Pleistocene rhyolitic center - sierra La Primavera, Jalisco, Mexico: Journal of Volcanology and Geothermal Research, v. 8, p. 199–230.

Mahood, G.A., 1981a, Chemical evolution of a Pleistocene rhyolitic center: Sierra La Primavera, Jalisco, Mexico: Contributions to Mineralogy and Petrology, v. 77, p. 129–149.

Mahood, G.A., 1981b, A summary of the geology and petrology of the Sierra La Primavera, Jalisco, Mexico: Journal of Geophysical Research, v. 86, p. 10137–10152.

Mahood, G.A., and Drake, R.E., 1982, K-Ar dating young rhyolitic rocks: A case study of the Sierra La Primavera, Jalisco, Mexico: Geological Society of America Bulletin, v. 93, p. 1232–1241.

Mahood, G., and Hildreth, W., 1983, Large partition coefficients for trace elements in high-silica rhyolites: Geochimica et Cosmochimica Acta, v. 47, p. 11–30.

Mahood, G.A., Truesdell, A.H., and Templos, M.L.A., 1983, A reconnaissance geochemical study of La Primavera geothermal area, Jalisco, Mexico: Journal of Volcanology and Geothermal Research, v. 16, p. 247–261.

Mahood, G.A., and Halliday, A.N., 1988, Generation of high-silica rhyolite: A Nd, Sr, and O isotopic study of Sierra La Primavera, Mexican Neovolcanic Belt: Contributions to Mineralogy and Petrology, v. 100, p. 183–191.

McKenzie, W.F., and Truesdell, A.H., 1977, Geothermal reservoir temperature estimated from the oxygen isotope compositions of dissolved sulfate and water from hot springs and shallow drillholes: Geothermics, v. 5, p. 51–61.

Michael, P.J., 1988, Partition coefficients for rare earth elements in mafic minerals of high silica rhyolites: The importance of accessory mineral inclusions: Geochimica et Cosmochimica Acta, v. 52, p. 275–282.

Nielsen, R.L., 1988, A model for the simulation of combined major and trace element liquid line of descent: Geochimica et Cosmochimica Acta, v. 52, p. 27–38.

Spera, F.J., Yuen, D.A., and Kirschvink, S.J., 1982, Thermal boundary layer convection in silicic magma chambers: Effects of temperature-dependent rheology and implications for thermogravitational chemical fractionation: Journal of Geophysical Research, v. 87, p. 8755–8767.

Stimac, J.A., Goff, F., and Wohletz, K., 2001, Thermal modeling of the Clear Lake magmatic-hydrothermal system, California, USA: Geothermics, v. 30, p. 349–390.

Tait, S.R., 1988, Samples from the crystallizing boundary layer of a zoned magma chamber: Contributions to Mineralogy and Petrology, v. 100, p. 470–483.

Valentine, G.A., 1992, Magma chamber dynamics, *in* Nierenberg, W.A. ed., Encyclopedia of earth system science, 3: New York, Academic Press, p. 1–17.

Verma, S.P., 1985a, Heat source in Los Humeros geothermal area, Puebla, Mexico: Geothermal Resources Council Transactions, v. 9, p. 521–525.

Verma, S.P., 1985b, On the magma chamber characteristics as inferred from surface geology and geochemistry: Examples from Mexican geothermal areas: Physics of the Earth and Planetary Interiors, v. 41, p. 207–214.

Verma, S.P., 2000, Geochemical evidence for a lithospheric source for magmas from Los Humeros caldera, Puebla, Mexico: Chemical Geology, v. 164, p. 35–60.

Verma, M.P., Verma, S.P., and Sanvicente, H., 1990, Temperature field simulation with stratification model of magma chamber under Los Humeros caldera, Puebla, Mexico: Geothermics, v. 19, p. 187–197.

Verma, S.P., and Andaverde, J., 1996, Temperature distributions from cooling of a magma chamber in Los Azufres geothermal field, Michoacán, Mexico: Geofísica Internacional, v. 35, p. 105–113.

Verma, S.P., and Rodríguez-González, U., 1997, Temperature field distribution from cooling of a magma chamber in La Primavera caldera, Jalisco, Mexico: Geothermics, v. 26, p. 25–42.

Verma, S.P., and Santoyo, E., 1997, New improved equations for Na/K, Na/Li and SiO_2 geothermometers by outlier detection and rejection: Journal of Volcanology and Geothermal Research, v. 79, p. 9–23.

Verma, S.P., and Andaverde, J., 2007, Coupling of thermal and chemical simulations in a 3-D integrated magma chamber-reservoir model: A new geothermal energy research frontier, *in* Ueckermann, H.I., ed., Geothermal energy research trends: New York, Nova Science Publishers, p. 149–189.

Verma, S.P., Pandarinath, K., and Santoyo, E., 2008, SolGeo: A new computer program for solute geothermometers and its application to Mexican geothermal fields: Geothermics, v. 37, p. 597–621.

Verma, S.P., and Díaz-González, L., 2011, Application of the discordant outlier detection and separation system in the geosciences: International Geology Review, doi: 10.1080/00206814.2011.569402.

Verma, S.P., Gómez-Arias, E., and Andaverde, J., 2011a, Thermal sensitivity analysis of emplacement of the magma chamber in Los Humeros caldera, Puebla, Mexico: International Geology Review, v. 53, p. 905–925.

Verma, S.P., Verma, S.K., Pandarinath, K., and Rivera-Gómez, M.A., 2011b, Evaluation of recent tectonomagmatic discrimination diagrams and their application to the origin of basic magmas in Southern Mexico and Central America: Pure and Applied Geophysics, doi: 10.1007/s00024-010-0173–2 (in press).

Villa Merlo, S.J., Chacón Franco, M., and Medina Orozco, G., 1987, Utilización de la relación atómica Na^+/K^+ para identificar zonas de mayor actividad hidrotermal en el campo geotérmico de la Primavera, Jalisco: Geotermia Revista Mexicana de Geoenergía, v. 3, p. 241–254.

White, D.E., 1970, Geochemistry applied to Discovery, evaluation, and exploitation of geothermal energy resource: Geothermics, special issue, p. 58–70.

Wright, J.V., 1981, The Rio Caliente ignimbrite: Analysis of a compound intraplinian ignimbrite from a major Late Quaternary Mexican eruption: Bulletin Volcanologique, v. 44, p. 189–212.

Yokoyama, I., and Mena, M., 1991, Structure of La Primavera caldera, Jalisco, Mexico, deduced from gravity anomalies and drilling results: Journal of Volcanology and Geothermal Research, v. 47, p. 183–193.

Bibliography

[1] Iglesias, E., Arellano, V., and Torres, R., 2005, Estmación del recurso y prospectiva tecnológica de la geotermia en México. Inform of the Electrical Research Institute: IIE/11/3753/I 01/P.

[2] Hardy, S., 2008, Structural evolution of calderas: Insights from two-dimensional discrete element simulations: Geology, v. 36, p. 927-930.

[3] Perugini, D., Poli, G., and Gatta, G.D., 2002, Analysis and simulation of magma mixing processes in 3D: Lithos, v. 65, p. 313-330.

[4] Yoshiaki, I., 2002, Computer simulation of time-dependent magma ascent processes involving bubbly and gassy flows: Journal of Volcanology and Geothermal Research, v. 196, p. 45-56.

[5] O'Sullivan, M.J., Pruess, K., and Lippmann, M., 2001, State of the art of geothermal reservoir simulation: Geothermics, v. 30, p. 395-429.

[6] Noorollahi, Y., and Itoi, R., 2011, Production capacity estimation by reservoir numerical simulation of northwest (NW) Sabalan geothermal field, Iran: Energy, v. 36, p. 4552-4569.

[7] Mottaghy, D., Pechnig, R., and Vogt, C., 2011, The geothermal project Den Haag: 3D numerical models for temperature prediction and reservoir simulation: Geothermics, v. 40, p. 199-210.

[8] Verma, S.P., and Andaverde, J., 2007, Coupling of thermal and chemical simulations in a 3-D integrated magma chamber-reservoir model: A new geothermal energy research frontier, in Ueckermann, H.I., ed., Geothermal energy research trends: New York, Nova Science Publishers, p. 149-188.

[9] Verma, S.P., Gómez-Arias, E., and Andaverde, J., 2011, Thermal sensitivity analysis of emplacement of the magma chamber in Los Humeros caldera, Puebla, Mexico: International Geology Review, v. 53, p. 905-925.

[10] Verma, S.P., Arredondo-Parra, U.C., Andaverde, J., Gmez-Arias, E., and Guerrero-Martínez, F.J., 2011, Three-dimensional temperature field simulation of a cooling

of a magma chamber, La Primavera caldera, Jalisco, Mexico: International Geology Review, doi: 10.1080/00206814.2011.585036 (in press).

[11] Viggiano-Guerra, J.C., Sandoval-Medina, F., Flores-Armenta, M.C, Pérez, R.J., and González-Partida, E., 2009, Aplicación del SPCALC en la especiación química y termodinámica de fluidos: ejemplo del caso de los pozos LV-4A, LV-11 y LV-13, del campo geotérmico de Las Tres Vírgenes, BCS: Geotermia: Revista Mexicana de Geoenergía,V.22, no. 1, p. 12-27.

[12] Demant, A., and Ortlieb, L., 1981, Plio-pleistocene volcano-tectonic evolution of la Reforma caldera, Baja California, Mexico: Tectonophysics, v. 71, p. 194.

[13] Garduño-Monroy, V.H., Vargas-Ledezma, H., and Campos-Enriquez, J.O., 1993, Preliminary geologic studies of Sierra El Aguajito (Baja California, Mexico): a resurgent-type caldera: Journal of Volcanology and Geothermal Research, v. 59, p. 47-58.

[14] Capra, L., Macías, J.L., Espíndola, J.M., and Siebe, C., 1998, Holocene plinian eruption of La Virgen volcano, Baja California, Mexico: Journal of Volcanology and Geothermal Research, v. 80, p. 239-266.

[15] López-Hernández, A., 1998, Síntesis geológica de la zona geotérmica de Las Tres Vírgenes, B.C.S., México: Geotermia, Revista Mexicana de Geoenergía, v. 14, no. 1, p. 3-14.

[16] Saunders, A.D., Rogers, G., Marriner, G.F., Terrell, D.J., and Verma, S.P., 1987, Geochemistry of Cenozoic volcanic rocks, Baja California, Mexico: implications for the petrogenesis of post-subduction magmas: Journal of Volcanology and Geothermal Research, v. 32, p. 223-245.

[17] Conly, A.G., Brenan, J.M., Hervé, B., and Scotta, S.D., 2005, Arc to rift transitional volcanism in the Santa Rosalía Region, Baja California Sur, Mexico: Journal of Volcanology and Geothermal Research, v. 142, p. 303-341.

[18] Angelier, J., Colletta, J., Chorowicz, L., Ortlieb, L., and Rangin, C., 1981, Fault tectonics of the Baja California Peninsula and the opening of the Sea of Cortez, Mexico: Journal of Structural Geology, v. 3, no. 4, p. 347-357.

[19] Schmitt, A.K., Stockli, D.F., Niedermann, S., Lovera, O.M., and Hausback, B.P., 2010, Eruption ages of Las Tres Vírgenes volcano (Baja California): A tale of two helium isotopes: Quaternary Geochronology, v. 5, no. 5, p. 503-511.

[20] Gutiérrez-Negrín, L.C.A., 1990, Litología, mineralogía y geotermometría del pozo LV-2, Las Tres Vírgenes, B.C.S: Geotermia: Revista Mexicana de Geoenergía, v. 6, no. 2, p. 185-211.

[21] Santoyo, E., García, A, Espinosa, G., González-Partida, E., and Viggiano, J.C., 2000, Thermal evolution study of the LV3 well in the Tres Vírgenes geothermal field, Mexico: World Geothermal Congress, Japan.

[22] Brueseke, M.E., and Hart, W.K., 2009, Intermediate composition magma production in an intracontinental setting: Unusual andesites and dacites of the mid-Miocene Santa Rosa-Calico volcanic field, Northern Nevada: Journal of Volcanology and Geothermal Research, v. 188, p. 197-213.

[23] Wohletz, K., Civetta, L., and Orsi, G., 1999, Thermal evolution of the Phlegraean magmatic system: Journal of Volcanology and Geothermal Research, v. 91, p. 381-414.

[24] Crisp, J.A., 1984, Rates of magma emplacement and volcanic output: Journal of Volcanology and Geothermal Research, v. 20, p. 177-211.

[25] Verma, S.P., and Rodríguez-González, U., 1997, Temperature field distribution from cooling of a magma chamber in La Primavera caldera, Jalisco, Mexico: Geothermics, v. 26, p. 25-42.

[26] Mahood, G.A., and Drake, R.E., 1982, K-Ar dating young rhyolitic rocks: A case study of the Sierra La Primavera, Jalisco, Mexico: Geological Society of America Bulletin, v. 93, p. 1232-1241.

[27] Mahood, G.A., Truesdell, A.H., and Templos, M.L.A., 1983, A reconnaissance geochemical study of La Primavera geothermal area, Jalisco, Mexico: Journal of Volcanology and Geothermal Research, v. 16, p. 247-261.

[28] Villa Merlo, S.J., Chacón Franco, M., and Medina Orozco, G., 1987, Utilización de la relación atómica Na+/K+ para identificar zonas de mayor actividad hidrotermal en el campo geotérmico de la Primavera, Jalisco: Geotermia Revista Mexicana de Geoenergía, v. 3, p. 241-254.

[29] Verma, S.P., Pandarinath, K., and Santoyo, E., 2008, SolGeo: A new computer program for solute geothermometers and its application to Mexican geothermal fields: Geothermics, v. 37, p. 597-621.

[30] Verma S.P. and Díaz-González, L., 2012, Application of the discordant outlier detection and separation system in the geosciences: International Geology Review, v. 54, no. 5, p. 593-614.

[31] Versteeg, H.K., and Malalasekera, W., 1995, An introduction to computational fluid dynamics: The finite volume method. Harlow, England, Pearson, Prentice Hall.

[32] Nielsen, R.L., 1988, A model for the simulation of combined major and trace element liquid line of descent: Geochimica et Cosmochimica Acta, v. 52, p. 27-38.

[33] Dobran, F., 2001, Volcanic processes: mechanisms in material transport, New York, U.S., Kluwer Academic/Plenum.

[34] Verma S.P., Kailasa, P., Santoyo, E., González-Partida, E., Torres-Alvarado, I.S., and Tello-Hinojosa, E., 2006, Fluid chemistry and temperatures prior to exploitation at the Las Tres Vírgenes geothermal field, Mexico: Geothermics, v. 35, p. 156-180.

[35] Andaverde, J., Verma, S.P., Santoyo, E., 2005, Uncertainty estimates of static formation temperatures in boreholes and evaluation of regression models: Geophysical Journal International, v. 160-3, p. 1112-1122.